



Numerical Analysis of Shallow Tunnels Under Static Loading: A Finite Element Approach

Mohammad Zaid · Swapnil Mishra

Received: 16 April 2020 / Accepted: 23 November 2020 / Published online: 3 January 2021
© Springer Nature Switzerland AG 2021

Abstract In the present world, the need for underground structures has grown many folds due to the increasing population, the advancement of public infrastructure, and the scarcity of land. Underground structures also provide attractive alternatives for storage of explosives and other military hardware. Being at shallow depth, their potential impact on the environment and surrounding structures can be significant. Therefore, it is crucial to understand the surrounding material behaviour for the safe and economical design of underground facilities. In the present work, an attempt is made to simulate the in situ condition using finite element, which has been validated by experimental results, to understand the tunnel deformation behaviour under static loading condition in soft rocks. 3D non-linear finite element analysis has been carried out by using Abaqus. Rockmass-tunnel model considered in this study has dimensions of 30 cm × 30 cm and 35 cm. The diameter of the tunnel has been varied from 2.5 cm, 3.5 cm to 5.0 cm. Similarly, the overburden depth is taken as 2.5 cm, 3.5 cm and 5.0 cm. Both the lined and unlined cases of

the tunnel have been considered. Geo-material has been prepared in the laboratory having four different compositions of POP, sand, clay and mica. The weathering effect of the rockmass is also considered in the study. Fresh, slightly weathered, medium weathered, and highly weathered are the four different weathering stages of basalt rock taken into consideration. The elasto-plastic behaviour is considered for the natural and synthetic rock, and a Mohr–Coulomb constitutive model is incorporated. Stress and deformation behaviour is monitored for different rocks and geo-materials. Longitudinal and transverse profiles of the tunnel have been plotted to understand the response of tunnel lining and the surrounding rockmass, along and across the point of loading. The paper concludes that the diameter of the tunnel, overburden depth of the tunnel, and weathering of rock has a significant effect on the stability of tunnels under severe loading conditions.

Keywords Basalt · Geo-material · Tunnel · Static loading · Finite element analysis

M. Zaid (✉)
Department of Civil Engineering, ZHCET, Aligarh
Muslim University, Aligarh, Uttar Pradesh 202002, India
e-mail: mohammadzaid1@zhcet.ac.in

S. Mishra
Department of Civil Engineering, PDPU, Gandhinagar,
Gujrat, India
e-mail: swapnil.mishra@sot.pdpu.ac.in

1 Introduction

The urbanisation and application of innovative construction practices all over the world have increased the vertical expansion of cities. The construction of

tunnels has become the most desired type of method for the faster system of transportation services (Meguid et al. 2008). However, the presence of complex geological surroundings, technological constraints, natural/artificial calamities such as downfall, the inrush of water, and excessive deformation often happens in the tunnel construction that degrades the serviceability and safety of tunnels (Li et al. 2013; Gao et al. 2018; Wang et al. 2019; Song et al. 2019). Several studies have been performed by various researchers and scientists to understand the stability of tunnels constructed in soil and rock media (Carranza-Torres and Fairhurst 1999; Ouchi et al. 2004). Most of the tunnels have been constructed through the geologically blocky and stratified structures having low in situ stresses (Moussaieia et al. 2019).

The experimental studies have been carried out to conclude that the span of the unsupported tunnel has a higher spacing ratio of vertical-horizontal discontinuities (Fuenkajorn and Phueakphum 2010). Besides, the stability of the unsupported span of the shallow tunnel is directly proportional to the dip on the unsupported span and the depth (Fuenkajorn and Phueakphum 2010). Moreover, (Jia and Tang 2008) used the rock failure process analysis (RFPA) code to study the effect of bedding-dip on tunnel stability. Furthermore, open zone, shear zone and failure zone have been found around the tunnel constructed in orthogonal discontinuous rockmass (Shen and Barton 1997). The deformation of underground openings has been evaluated for different dimensions of openings (Jiang et al. 2006). The small-scaled model study was carried out by Moyo and Stacey (2012), to understand the mechanics of rock bolting in jointed rockmass for deep mining.

De Buhan et al. (1999) carried out the stability analysis of the shallow tunnel face when excavated below a water table. It was concluded that the water seepage pressure significantly affects the stability of shallow tunnels. Gioda and Cividini (1996) studied the tunnelling in rocks containing clay mineral using a numerical method of analysis. The swelling and squeezing behaviour was observed in the rock tunnels, and consequently, linear-nonlinear constitutive models were found suitable for carrying out the finite element analysis for creep. Manouchehrian and Cai (2017) studied the effect of static and dynamic loading due to high-stress fields present inside the tunnel. They concluded that the presence of geological structures in

the proximity of tunnels influences the rock bursting. However, they did not consider the relationship between the static loading variation and deformation for the tunnel in the rock. The existing patterns of joint-sets have a considerable influence on the stability of the tunnel, but the presence of tectonic stresses dominates the failure effect in the tunnel (Jia and Tang 2008).

The damage inside the tunnel is caused as a result of the load from the superstructure, overburden weight, in situ stresses and other factors. The deformation measures the magnitude of damage in the tunnel and proves to be an essential parameter in tunnel health monitoring. The elastic and plastic failure of weak rock was studied by Sakurai (1983) for the loading and unloading cases. It was concluded that deformation is unrecoverable for the plastic failure of rock for an unloading condition. The circular shape of the tunnels is preferred in case of weak/soft ground due to the ability of circular shape to readjust to subsequent load changes and inherently has higher strength (Mishra et al. 2018). The basic engineering properties, such as uniaxial compressive strength, water softening, Young's modulus, bulk modulus and Poisson's ratio have a significant effect on the deformations in the rock (Mishra et al. 2018). An experimental study was carried out by Gupta (1997) to classify different rocks based on the degree of weathering. It was concluded that the strength parameters are affected by the degree of weathering and reduces the strength of rock.

Several researchers have carried out the stability analysis of tunnel under static loading (Athar et al. 2019; Zaid et al. 2019c, 2020a; Naqvi et al. 2020). Chehade and Shahrour (2008) had studied the effect of alignment between the twin tunnel. They concluded that the maximum settlement is observed for vertically aligned tunnels, and minimum settlement is observed for the horizontally aligned tunnel. Zangerl et al. (2008) analysed the consolidation settlement behaviour on the ground above deep tunnels in fractured crystalline rock. It was determined that the pore water pressure of the crystalline rock had a direct influence on the consolidation settlement above the tunnel. Moreover, the significant amount of settlement was observed that affected the serviceability of the tunnel. Several researchers have studied the behaviour of rock tunnels and other underground structures using different approaches for better understanding of underground spaces constructed in rocks (Gahoi et al. 2017;

Naqvi et al. 2017; Fakhimi et al. 2018; Ali Khan et al. 2019; Zaid et al. 2019a, b, 2020b; Zaid and Sadique 2020a, b, c, d; Zaid and Rehan Sadique 2021). The finite element method (FEM) (Sterpi and Cividini 2004; Kasper and Meschke 2004) or finite difference method (FDM) (Senent and Jimenez 2015; Zhao et al. 2015) have been widely used to study the stress distribution and deformation in the rock tunnel.

In the present paper, the authors have carried out a three-dimensional non-linear analysis of tunnel excavated through rock and geo-material. The finite element technique has been used for the different analyses under the static loading condition. The deformation patterns and stresses in different cases have been discussed in detail for the effect of diameter of the tunnel, overburden depth, degree of weathering and magnitude of the load. Moreover, the deformation patterns have been plotted along the length of the tunnel for the evaluation of longitudinal deformation. Afterwards, an analytical relation has been derived for the deformation profile of different rocks and geo-materials considered in the present study.

2 Numerical Analysis

2.1 Finite Element Model

The 3D finite element geometry has been modelled by using Abaqus, which is based on a continuum mechanics approach of analysis. The finite element model of the rock and geo-material surrounding the tunnel has 0.30 m (width) \times 0.30 m (height) \times 0.35 m (length) of geometrical dimensions (Mishra et al. 2016, 2018). The diameter of the tunnel is varied as 0.025 m, 0.035 m and 0.05 m and an overburden depth of 0.025 m, 0.035 m, and 0.05 m has been considered for each diameter tunnel. Both lined and unlined tunnels have been considered for each diameter and overburden depth of the different rocks and geo-materials. The diameter and height of a loading patch are 0.05 m and 0.05 m respectively, and it has been placed at the middle length of the tunnel on the top surface. The geometry of the model and its meshing for different cases are shown in Figs. 1 and 2.

The scaling of the model is useful in relating the behaviour of the small-scale model with the prototype model. For the simplified representation, the values of Young's modulus, Poisson's ratio and density in the

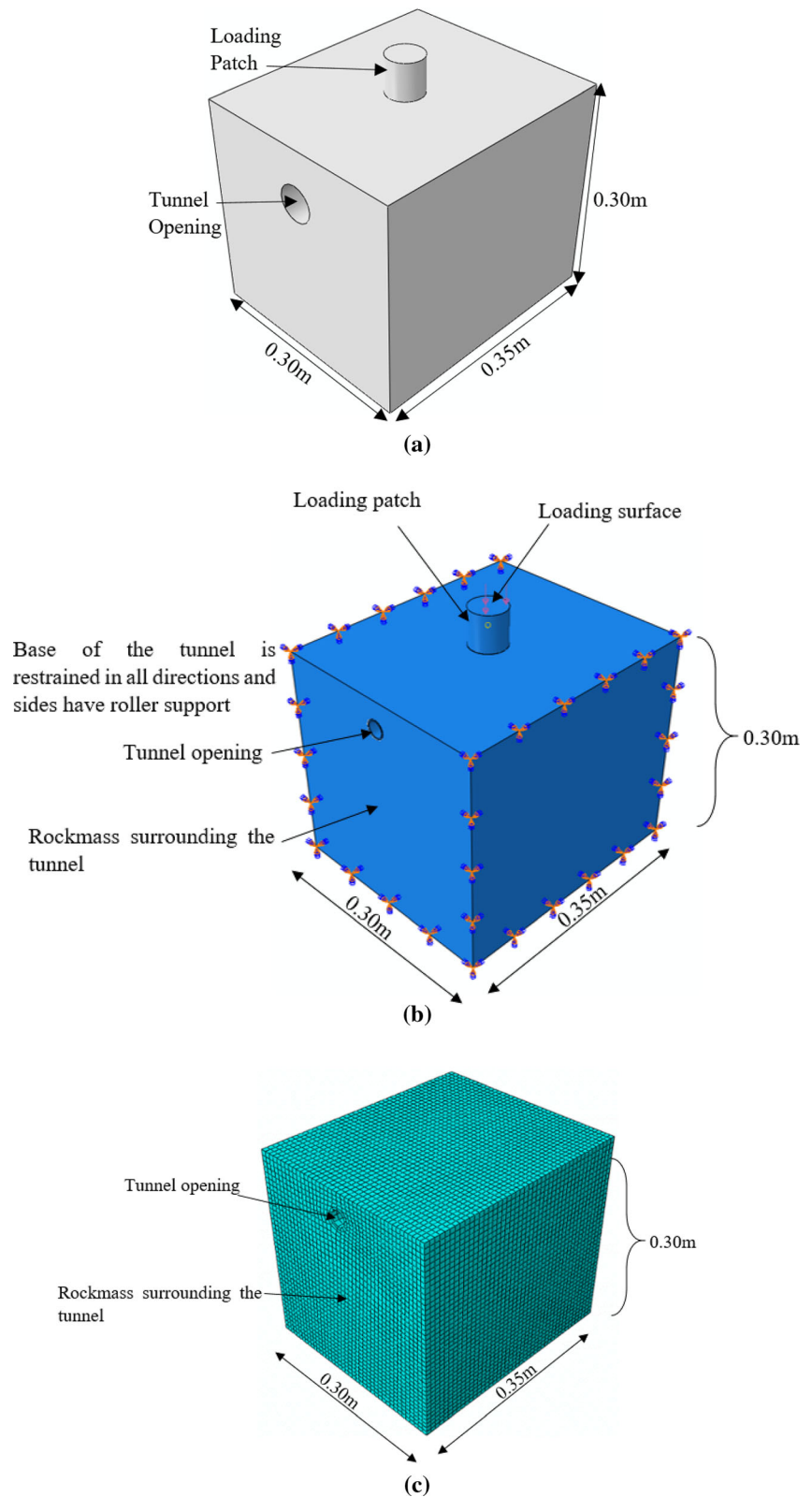
small-scaled model are assumed to be same as of prototype models. Further, the external loads have been represented through homogeneous points, to satisfy the requirement of the geometrically similar scaling. The dimensions of the geometry of the rock and geomaterial tunnel model, lining thickness and mesh size have been reduced by 100 times of prototype model.

The site of railway tunnel project at, T-48 Quazigund tunnel in Katra, Jammu has been considered as a prototype, from where the properties of surrounding rockmass and tunnel lining are chosen for fixing the model specifications (Mishra et al. 2020). To represent in situ weak and weathered rocks at shallow depths, the ratio of elastic modulus of lining material to the elastic modulus of surrounding rock ($E_{\text{lining}}/E_{\text{rock}}/\text{geomaterial}$) has been kept constant for model studies. The rockmass present at the T-48 Quazigund tunnel consists of the Carbonaceous Phyllite and Quartzitic Phyllite. The elastic modulus (E_{rock}) of carbonaceous Phyllite has been reported as 33.00 GPa (Mishra et al. 2020). As far as the lining is concerned, shotcreting was done using M-30 grade concrete. The elastic modulus of the lining material is reported to be 27.39 GPa. It was found that the elastic modulus ratio calculated from field data was 0.83 (Mishra et al. 2020). The approximate value of the elastic modulus of lining used in physical modelling is determined using the following equation:

$$\left(\frac{E_{\text{lining}}}{E_{\text{rock/geomaterial}}} \right)_{\text{Scaledmodel}} = \left(\frac{E_{\text{lining}}}{E_{\text{rock/geomaterial}}} \right)_{\text{Prototypemodel}} \quad (1)$$

Further, the selection of lining material and thickness of lining used for physical modelling has been decided based on the proper scaling of the structural interaction of real field conditions. Finally, PVC hollow tube was selected as a lining material for scaled studies. The lining thickness of tunnel was fixed by comparing the ratio of lining thickness with tunnel diameter of real field condition and physical modelling. The ratio of lining thickness and tunnel diameter of T-48 railway tunnel project gives a constant value, which has been equated with the ratio of lining thickness and tunnel diameter of the physical model. Since the diameter of the model is already assumed and fixed, hereafter, the thickness of the

Fig. 1 Different parts of numerical model
a Geometry of the tunnel model of present study,
b Assembly of the finite element model,
c Tunnel meshed model,
d Tunnel lining meshed model,
e Meshing of loading patch,
f 0.025 m, **g** 0.035 m, and **h** 0.050 m of overburden depth



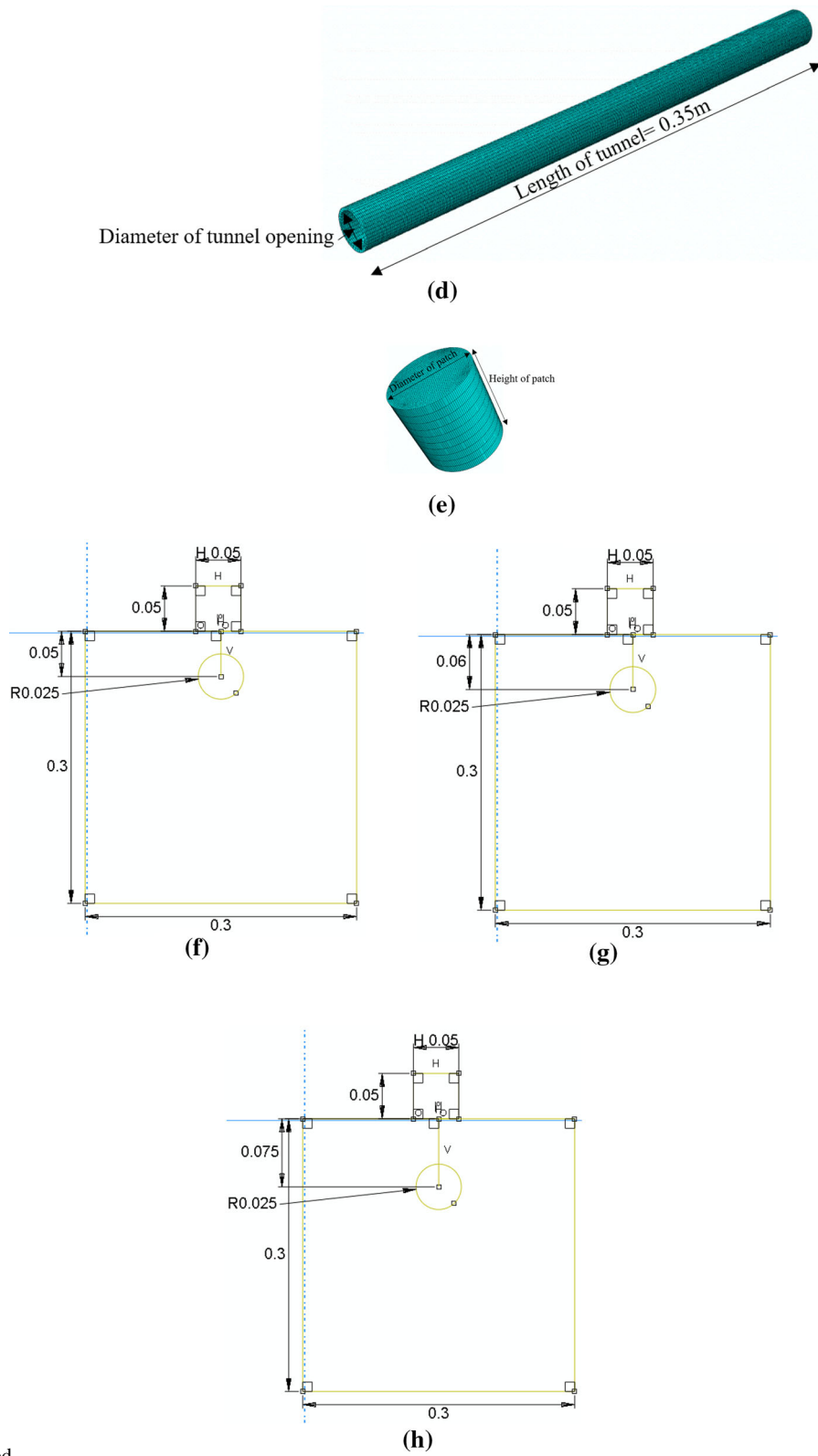


Fig. 1 continued

Table 1 Scaling of the different parameters of the model

Parameter	Model value where prototype is 1.0	Unit
Length	1/N	m
Velocity	1	m/s
Pressure	1	MPa
Deformation	1	m

tunnel lining has been computed. Tables 1 and 2 represents the description related to the scaling of the model adopted in the present paper for rock and geomaterial models of the tunnel.

2.2 Constitutive Material Model

2.2.1 Material Model for Different Geo-Materials and Rocks

The rocks and geo-materials are governed by the Mohr–Coulomb plasticity model that allows the material to harden or soften isotropically (Abaqus 2014; Systemes 2014). The yield criterion of Mohr–Coulomb plasticity model is represented as

$$\tau = c + \sigma \tan \phi \tag{2}$$

where τ is shear strength, c is cohesion, σ is normal stress, and ϕ is an internal friction angle of the rock. For the general state of stress, the Mohr–Coulomb model has three stress invariants which are given as

$$F = R_{mc}q - p \tan \phi - c = 0 \tag{3}$$

where,

$$R_{mc}(\Theta, \phi) = \frac{1}{\sqrt{3} \cos \phi} \sin\left(\Theta + \frac{\pi}{3}\right) + \frac{1}{3} \cos\left(\Theta + \frac{\pi}{3}\right) \tan \phi \tag{4}$$

$$\cos(3\Theta) = \left(\frac{r}{q}\right)^3 \tag{5}$$

$$p = -\frac{1}{3} \text{trace}(\sigma) \tag{6}$$

$$q = \sqrt{\frac{3}{2}} (S : S) \tag{7}$$

$$r = (9(S * S : S))^{\frac{1}{3}} \tag{8}$$

$$S = \sigma + pI \tag{9}$$

where Θ represents a deviatoric polar angle, p is the equivalent pressure stress, q is the Mises equivalent stress, r is the third invariant of deviatoric stress, S is the deviatoric stress.

Further, the flow potential, G for Mohr–Coulomb yield surface is represented as

$$G = \sqrt{(\varepsilon c|_0 \tan \psi)^2 + (R_{mw}q)^2} - p \tan \psi \tag{10}$$

where,

$$R_{mw}(\Theta, e) = \frac{4(1 - e^2) \cos^2 \Theta + (2e - 1)^2}{2(1 - e^2) \cos \Theta + (2e - 1) \sqrt{4(1 - e^2) \cos^2 \Theta + 5e^2 - 4e}} R_{mc}\left(\frac{\pi}{3}, \phi\right) \tag{11}$$

and,

$$R_{mc}\left(\frac{\pi}{3}, \phi\right) = \frac{3 - \sin \phi}{6 \cos \phi} \tag{12}$$

where ψ is the dilation angle measured in the $p - R_{mw}q$ plane at high confining pressure, $c|_0$ is the initial cohesion yield stress, $c|_0 = c|_{\varepsilon} pI = 0$, ε is meridional eccentricity, e is a parameter, referred to as the deviatoric eccentricity.

The deviatoric eccentricity, e , is calculated as

$$e = \frac{3 - \sin \phi}{3 + \sin \phi} \tag{13}$$

In this study, four different rocks and geo-materials have been considered for the analysis of different cases. Moreover, a Plaster of Paris (POP) has been considered in this paper for the evaluation of laboratory model. Furthermore, geo-material-1, geo-material-2, geo-material-3 and geo-material-4 are the four different geo-materials that have been considered in the analyses. These geo-materials were prepared with different composition ratios of POP, sand and clay, and the preparation details were discussed by Mishra et al. (2016), Mishra (2019). The geo-material-1, 2, 3 and 4 have composition of POP (50%); sand (35%); clay (15%), POP (80%); clay (20%), POP (50%); sand (30%); clay (20%), and POP (50%); sand (20%); clay (30%) (by weight) respectively. The properties of the geomaterials and POP are taken from Mishra (2019).

Table 2 Details related to dimensions of the scaled model adopted in the present study

Rock-tunnel Model		Small scale model	Prototype
Dimension	Surrounding rock mass	30 cm × 30 cm × 35 cm	30 m × 30 m × 35 m
	Tunnel	Length 35 cm, Diameter 5 cm	Length 35 m, Diameter 5 m

Table 3 Input Properties for Numerical Model (Gupta 1997; Mishra et al. 2017; Zaid et al. 2021; Mishra 2019)

Rock type	Density (kg/m ³)	Young's modulus (GPa)	Poisson's ratio	Cohesion (MPa)	Friction angle (°)	UCS (MPa)
<i>Fresh Basalt</i>	2960	46.510	0.187	26.250	63.38	172.55
<i>Slightly Weathered Basalt</i>	2790	20.630	0.260	18.500	53.71	93.20
<i>Medium Weathered Basalt</i>	2560	2.770	0.272	8.080	43.87	17.80
<i>Highly Weathered Basalt</i>	2120	0.630	0.272	1.640	33.33	3.40
<i>Geo-material-1</i>	1410	4.260	0.160	1.810	42.00	4.48
<i>Geo-material-2</i>	1220	3.675	0.163	0.790	39.12	3.74
<i>Geo-material-3</i>	1094	2.810	0.216	0.627	31.40	1.38
<i>Geo-material-4</i>	1106	2.481	0.277	0.400	22.65	1.21
<i>POP</i>	1170	4.480	0.220	0.880	44.00	6.78
<i>Patch</i>	7800	210.000	0.330	–	–	–
<i>Lining</i>	1400	2.000	0.350	–	–	–

Further details about the geo-material preparation and testing have been discussed by Mishra et al. (2016).

Moreover, the properties of the rocks corresponding to the different degree of weathering is considered from Gupta (1997), Mishra et al. (2017), Zaid et al. (2019a, 2021), which is presented in Table 3. The basalt rock included in the present work has four different weathering degrees, mainly fresh, slightly weathered, medium weathered and highly weathered. Several researchers studied the effect of weathering on the stability of structures constructed in basalt rock (Gahoi et al. 2017; Athar et al. 2019; Zaid et al. 2019a). Further, the elastoplastic properties of different stages of weathering of basalt were studied by Gupta (1997).

2.2.2 Material Model For Loading Patch And Tunnel Lining

The material of the loading patch and tunnel lining, based on the previous studies, has been assumed as

elastic (Mishra et al. 2016). The loading patch and lining of the tunnel has a density of 7800 kg/m³ and 1400 kg/m³ respectively, Young's modulus of 210 GPa and 2.0 GPa respectively and Poisson's ratio of 0.33 and 0.35 respectively.

2.3 Boundary Conditions

Figure 1b shows the boundary conditions adopted in the present study for the numerical model. The base of the finite element model has been fixed in x, y, and z directions. The vertical boundaries of the rock model were restrained, and roller supports were applied. The loading patch has been placed at the ground surface above the crown of the tunnel. The load has been applied on the top surface of the loading patch having the magnitude equal to the UCS of surrounding rock/geo-material. Moreover, the load is applied in the form of uniformly distributed pressure, and its value has been varied from zero percent of UCS to hundred percent of UCS. In the present case, the

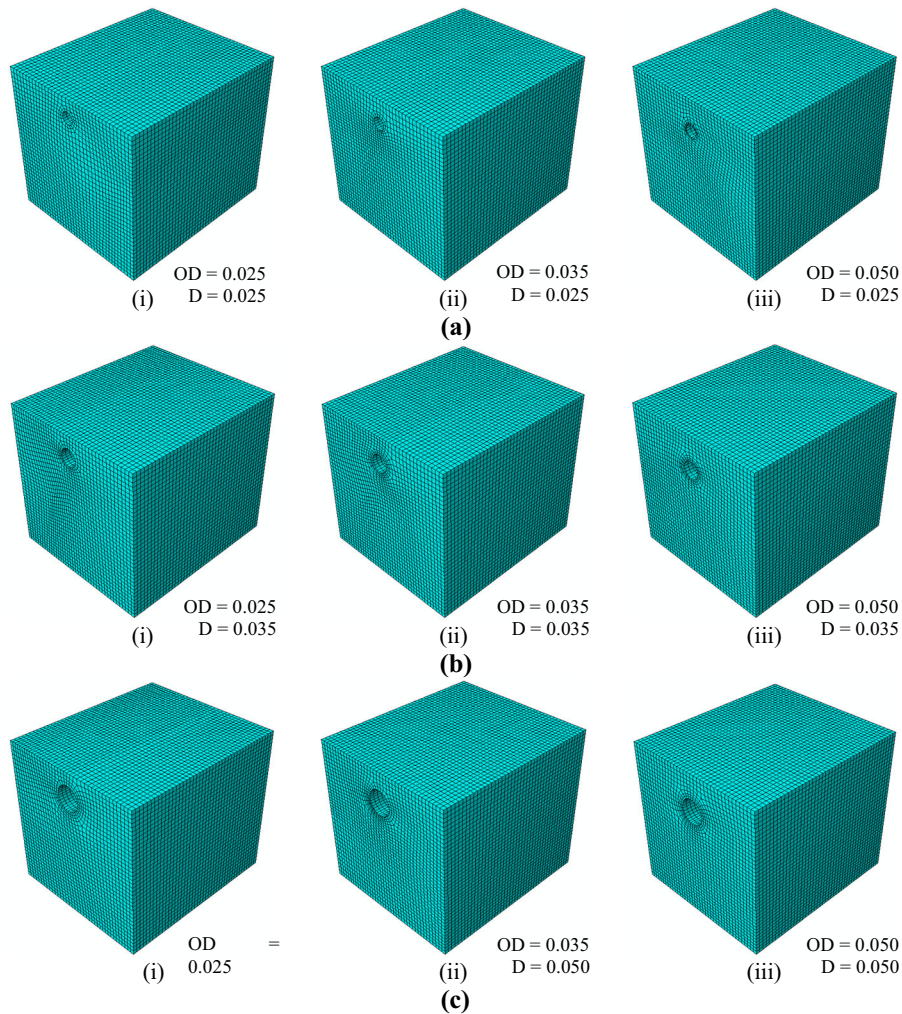


Fig. 2 Meshed models of different cases of tunnel having overburden depths (OD) of (i) 0.025 m, (ii) 0.035 m, and (iii) 0.050 m and diameter (D) of tunnel are **a** 0.025 m, **b** 0.035 m and **c** 0.050 m

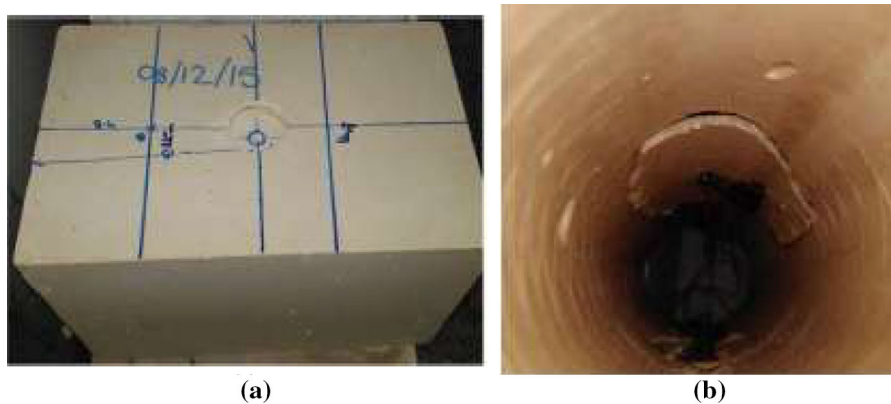
applied load is equal to the UCS of rock/geomaterial surrounding the tunnel. Afterwards, the applied load is 95% of the UCS value in the second analysis of the same finite element model. The load, in later cases, is varied by reducing the value of UCS (pressure) at an interval of 5%. The analysis has been carried out similarly for all the different cases. Therefore, first analysis for a rock/geo-material has been carried out for 100% of UCS (pressure) till the load is 0% of UCS, i.e., the case of “NO LOAD APPLIED”. The hard contact option has been applied in the interaction property module of Abaqus. The penalty contact has been assigned between the tunnel lining and internal surface of the rock/geo-material.

2.4 Meshing of Model Parts

The mesh convergence study has been carried out to estimate the size of an element for different parts of the finite element model. The parts of the model presented in Figs. 1 and 2 shows the meshing of the parametric study models. The mesh convergence study has been carried out to obtain an optimum mesh size. The deformation caused by the application of load through the loading patch has been observed at the crown of the tunnel. The element size of mesh for rock has been considered as 0.030, 0.020, 0.010, 0.009, 0.006, 0.003, 0.001, 0.0015, 0.0010, and 0.0005, the deformation observed for the varying element sizes as 0.0547 m, 0.0566 m, 0.0583 m, 0.0612 m, 0.0654 m, 0.0685 m,

Table 4 Validation of experimental and numerical method

Parameter	Experimental (Mishra et al. 2017; Mishra 2019)		Present study	
	Geomaterial	POP	Geomaterial	POP
Crack length along the tunnel axis (in mm)	97.00	85.00	95.00	0.81
Crack length transverse to the tunnel axis (in mm)	41.00	34.00	37.00	31.00
Crown Deformation (in mm)	0.37	0.30	0.34	0.28

**Fig. 3** Deformed shape of the geo-material model **a** top view and **b** internal view

0.0725 m, 0.0731 m, 0.0743 m, 0.07432 m, and 0.074322 m respectively. A minimal change in the value of deformation has been observed after the element size of 0.0015 m, therefore, the element size for the rock/geo-material, lining and loading patch has been considered as 0.0015 m, 0.0010 m, and 0.0010 m respectively. The present finite element model has been meshed by using C3D8R linear hexahedron element type. The C3D8R element type can be defined as an 8-noded linear brick element having reduced integration with hourglass control.

3 Validation of the Numerical Model

The finite element model of the tunnel under the static loading condition has been validated with the experimental results as reported by Mishra et al. (2016, 2017). The present validation has incorporated all the boundary conditions and loading conditions as given in previously published literature. The validation model has the dimensions as 0.30 m × 0.30 m × 0.35 m. It has a diameter of 0.05 m and overburden depth of 0.05 m. The Mohr–Coulomb elastoplastic

constitutive model has been considered in the validation of numerical analysis with experimental results. The material model has a density = 1410 kg/m³, unconfined compressive strength = 4.48 MPa, Young's modulus = 3.153GPa and Poisson's ratio = 0.16. The material in which the tunnel model was made has cohesion and friction angle value as 0.79 MPa and 39°. The load has been applied through the loading patch, which is placed at the top surface of the tunnel model. The validation results have been presented in Table 4. Mishra et al. (2016) and Mishra (2019) have discussed further detailed demonstration about the sample preparation, material strength determination and method of testing. Figure 3 shows the experimental test result when the sample was tested at the laboratory models.

4 Results and Discussion

The finite element analysis of shallow tunnels has been carried out in the present study using Abaqus. The tunnel was subjected to the static loading through the loading patch in the form of pressure, and the value of

pressure has been varied as a percentage of UCS. The 0% reduction in pressure magnitude stands for a condition when pressure has magnitude equal to UCS value of rock/geo-material surrounding the tunnel. The overburden depth and diameter of the tunnel has been considered as 0.025 m, 0.035 m and 0.050 m for both the cases. The present study has been carried out to understand the relation between the static load applied, overburden depth, a diameter of the tunnel and the degree of weathering of the shallow depth tunnel.

Table 5 shows the deformations obtained by varying the magnitude of the load on different rocks and geo-materials considering the degree of weathering in case of lined tunnels. The load has been varied by reducing the value of UCS (pressure) by an interval of 5%, initially at 0% reduction (pressure = UCS) to 100% reduction (pressure = 0 kPa) for the different rocks and geo-materials having different geometrical configurations. A 5% reduction in magnitude of pressure (equal to 0.95UCS) has been applied, and the analysis has been carried out till 100% reduction in the pressure (pressure = 0 kPa). The deformation corresponding to the reduction in the percentage of UCS for different rocks considered in the present study is shown in Table 5 for the case of 0.05 m diameter and 0.025 m overburden depth. Table 5 illustrates that the deformation increases with the increase in the degree of rock weathering, which was also depicted by the geo-materials prepared in the laboratory for simulating the weathering. As the strength of geo-material reduces from geo-material-1 to geo-material-2, the deformation increased by 45% and similarly, the deformation increased by 87% when the grade of geo-material changes from geo-material-2 to geo-material-3 and geo-material-3 to geo-material-4, when pressure was at 0% reduction in UCS. From Table 5, it can be concluded that the magnitude of deformation increases from 6% to 50% of the former rock/geo-material for the reduction in percentage of UCS, for the same material.

Furthermore, Table 6 and 7 have been plotted for an overburden depth of 0.035 m and 0.050 m respectively having 0.05 m of tunnel diameter with lining. The magnitude of pressure has been varied is similar to the previous cases in terms of percentage of UCS value of rock/geo-material in which tunnel has been constructed. In this case, it has been observed that the deformation increases with a decrease in the

Table 5 Comparison of deformation in different rocks for 0.05 m diameter Lined tunnel having 0.025 m overburden depth ($\times 10^{-2}$ m) to understand the effect of pressure in terms of percentage reduction of UCS

Rock	0%	5%	10%	15%	20%	25%	30%	35%	40%	45%	50%	55%	60%	65%	70%	75%	80%	85%	90%	95%	100%	
0.025 m overburden depth																						
Geo-material																						
1	0.0912	0.0858	0.0805	0.0753	0.0702	0.0651	0.0602	0.0553	0.0505	0.0458	0.0410	0.0366	0.0320	0.0275	0.0231	0.0188	0.0148	0.0110	0.0087	0.0073	0.0000	
2	0.2029	0.1916	0.1808	0.1701	0.1596	0.1492	0.1390	0.1288	0.1186	0.1086	0.0985	0.0887	0.0788	0.0690	0.0592	0.0493	0.0395	0.0296	0.0198	0.0099	0.0001	
3	0.2341	0.2225	0.2110	0.1994	0.1878	0.1763	0.1647	0.1531	0.1415	0.1299	0.1183	0.1066	0.0950	0.0834	0.0717	0.0601	0.0484	0.0367	0.0250	0.0133	0.0005	
4	0.2704	0.2569	0.2434	0.2300	0.2165	0.2030	0.1895	0.1760	0.1625	0.1491	0.1356	0.1221	0.1086	0.0951	0.0816	0.0680	0.0545	0.0410	0.0275	0.0140	0.0016	
POP	1	0.0743	0.0687	0.0636	0.0589	0.0544	0.0502	0.0463	0.0427	0.0392	0.0357	0.0324	0.0291	0.0258	0.0226	0.0194	0.0162	0.0130	0.0098	0.0066	0.0034	0.0002
Basalt	1	0.0199	0.0189	0.0180	0.0170	0.0160	0.0150	0.0140	0.0130	0.0121	0.0111	0.0101	0.0091	0.0081	0.0071	0.0062	0.0052	0.0042	0.0032	0.0022	0.0012	0.0003
	2	0.0299	0.0284	0.0269	0.0254	0.0239	0.0225	0.0210	0.0195	0.0180	0.0165	0.0151	0.0136	0.0121	0.0106	0.0091	0.0076	0.0062	0.0047	0.0032	0.0017	0.0002
	3	0.0408	0.0386	0.0365	0.0344	0.0323	0.0302	0.0282	0.0261	0.0241	0.0222	0.0202	0.0180	0.0162	0.0142	0.0122	0.0102	0.0082	0.0062	0.0042	0.0022	0.0002
	4	0.0593	0.0564	0.0534	0.0505	0.0475	0.0446	0.0416	0.0387	0.0357	0.0328	0.0298	0.0268	0.0239	0.0209	0.0180	0.0150	0.0121	0.0091	0.0062	0.0032	0.0003

Table 6 Comparison of deformation in different rocks for 0.05 m diameter *Lined* tunnel having 0.035 m overburden depth ($\times 10^{-2}$ m) to understand the effect of pressure in terms of percentage reduction of UCS

Rock	0%	5%	10%	15%	20%	25%	30%	35%	40%	45%	50%	55%	60%	65%	70%	75%	80%	85%	90%	95%	100%	
0.035 m overburden depth																						
Geo-material	1	0.0865	0.0809	0.0754	0.0699	0.0646	0.0596	0.0545	0.0496	0.0449	0.0406	0.0364	0.0324	0.0284	0.0246	0.0210	0.0173	0.0138	0.0103	0.0069	0.0035	0.0000
	2	0.1798	0.1706	0.1614	0.1523	0.1433	0.1343	0.1253	0.1164	0.1074	0.0985	0.0895	0.0806	0.0716	0.0627	0.0537	0.0448	0.0359	0.0269	0.0180	0.0090	0.0001
	3	0.2082	0.1979	0.1876	0.1773	0.1670	0.1567	0.1464	0.1361	0.1258	0.1155	0.1051	0.0948	0.0845	0.0741	0.0638	0.0534	0.0431	0.0327	0.0224	0.0120	0.0004
	4	0.2369	0.2251	0.2133	0.2015	0.1897	0.1779	0.1660	0.1542	0.1424	0.1306	0.1187	0.1069	0.0951	0.0833	0.0714	0.0596	0.0478	0.0360	0.0241	0.0123	0.0016
POP	1	0.0589	0.0556	0.0524	0.0493	0.0462	0.0432	0.0403	0.0374	0.0345	0.0316	0.0287	0.0259	0.0230	0.0202	0.0173	0.0144	0.0116	0.0087	0.0059	0.0030	0.0002
Basalt	1	0.0174	0.0169	0.0161	0.0149	0.0140	0.0131	0.0123	0.0114	0.0106	0.0097	0.0088	0.0080	0.0071	0.0063	0.0054	0.0045	0.0037	0.0028	0.0021	0.0012	0.0003
	2	0.0266	0.0253	0.0240	0.0227	0.0213	0.0200	0.0187	0.0174	0.0161	0.0147	0.0134	0.0121	0.0108	0.0095	0.0081	0.0068	0.0055	0.0042	0.0029	0.0016	0.0002
	3	0.0363	0.0345	0.0327	0.0309	0.0290	0.0272	0.0254	0.0236	0.0218	0.0200	0.0182	0.0164	0.0146	0.0128	0.0110	0.0092	0.0074	0.0056	0.0038	0.0021	0.0002
	4	0.0536	0.0510	0.0483	0.0456	0.0430	0.0403	0.0376	0.0350	0.0323	0.0296	0.0269	0.0243	0.0216	0.0189	0.0163	0.0136	0.0109	0.0083	0.0056	0.0029	0.0002

Table 7 Comparison of deformation in different rocks for 0.05 m diameter *Lined* tunnel having 0.050 m overburden depth ($\times 10^{-2}$ m) to understand the effect of pressure in terms of percentage reduction of UCS

Rock	0%	5%	10%	15%	20%	25%	30%	35%	40%	45%	50%	55%	60%	65%	70%	75%	80%	85%	90%	95%	100%	
0.05 m overburden depth																						
Geo-material	1	0.0769	0.0715	0.0660	0.0612	0.0564	0.0519	0.0477	0.0437	0.0399	0.0361	0.0325	0.0289	0.0255	0.0221	0.0189	0.0157	0.0125	0.0094	0.0063	0.0031	0.0000
	2	0.1638	0.1555	0.1472	0.1390	0.1307	0.1225	0.1143	0.1061	0.0980	0.0898	0.0816	0.0735	0.0653	0.0572	0.0490	0.0409	0.0327	0.0245	0.0164	0.0082	0.0001
	3	0.1914	0.1819	0.1724	0.1629	0.1535	0.1440	0.1345	0.1250	0.1155	0.1060	0.0966	0.0871	0.0776	0.0681	0.0586	0.0491	0.0396	0.0301	0.0206	0.0111	0.0004
	4	0.2165	0.2057	0.1949	0.1841	0.1733	0.1625	0.1517	0.1409	0.1301	0.1193	0.1085	0.0977	0.0869	0.0761	0.0653	0.0545	0.0437	0.0329	0.0221	0.0113	0.0016
POP	1	0.0532	0.0505	0.0477	0.0450	0.0423	0.0396	0.0369	0.0342	0.0316	0.0289	0.0263	0.0237	0.0210	0.0184	0.0158	0.0132	0.0106	0.0080	0.0054	0.0028	0.0001
Basalt	1	0.0159	0.0151	0.0144	0.0136	0.0128	0.0120	0.0112	0.0104	0.0097	0.0089	0.0081	0.0073	0.0065	0.0057	0.0050	0.0042	0.0034	0.0026	0.0018	0.0010	0.0003
	2	0.0243	0.0231	0.0219	0.0207	0.0195	0.0183	0.0171	0.0159	0.0147	0.0135	0.0123	0.0111	0.0099	0.0087	0.0072	0.0063	0.0050	0.0038	0.0026	0.0014	0.0002
	3	0.0333	0.0316	0.0299	0.0283	0.0266	0.0249	0.0233	0.0216	0.0200	0.0183	0.0167	0.0150	0.0134	0.0117	0.0101	0.0084	0.0068	0.0051	0.0035	0.0018	0.0002
	4	0.0491	0.0467	0.0442	0.0418	0.0393	0.0369	0.0344	0.0320	0.0296	0.0271	0.0247	0.0222	0.0198	0.0173	0.0149	0.0125	0.0100	0.0076	0.0051	0.0027	0.0002

magnitude of UCS (pressure). However, it ranges between 6% to 50% increase in comparison to deformation in the former case. Therefore, it has been observed that the magnitude of deformation and UCS are linearly proportional to each other, irrespective of the overburden depth, tunnel diameter and degree of weathering. However, the degree of weathering increases the amount of damage in the tunnel, and therefore, the tunnel stability reduces with an increase in the degree of weathering. Hence, the stability of the tunnel is inversely proportional to the degree of weathering.

Tables 8, 9, and 10 are presented to show the variation of deformation in unlined tunnels having 0.025 m, 0.035 m and 0.05 m overburden depth respectively in the case of 0.050 m of tunnel diameter for different weathering stages of basalt rock and geo-materials. It has been observed from Tables 8, 9, and 10, that the lined and unlined tunnel cases have similar behaviour when the pressure is varied for the different cases of overburden depth and diameter of the tunnel. However, the maximum change in the deformation has been observed in the case of the unlined tunnel, i.e., 90%, when the pressure changes from 90% of UCS to 95%. Moreover, the stability of lined and unlined tunnels increased with an increase in the overburden depth and decrease in the diameter of the tunnel as reported from Tables 8, 9, and 10. Also, the deformation increases with decrease in the overburden depth of tunnel or vice versa. Therefore, Tables 8, 9, and 10 conclude that the deformation is inversely proportional to the overburden depth and directly proportional to the magnitude of the pressure.

Figure 4 shows the deformation profiles of the lined tunnel constructed in the fresh, slightly weathered, medium weathered and highly weathered basalt rocks and geo-material-(1, 2, 3 & 4) having overburden depth of 0.025 m, 0.035 m and 0.050 m. It has been observed that the magnitude of deformation increases with the degree of weathering and therefore, has a directly proportional relationship with the degree of weathering. The tunnels constructed in fresh rock/geo-material (no weathering) have higher safety and serviceability due to lesser magnitude of deformations. However, a higher magnitude of damage has been observed in the tunnels constructed in the highly weathered stage. Therefore highly weathered rock and geo-material have lesser serviceability. Figure 4a–c have been plotted for an overburden depth of 0.025 m,

Table 8 Comparison of deformation in different rocks for 0.05 m diameter *Unlined* Tunnel having 0.025 m overburden depth ($\times 10^{-2}$ m) to understand the effect of pressure in terms of percentage reduction of UCS

Rock	0%	5%	10%	15%	20%	25%	30%	35%	40%	45%	50%	55%	60%	65%	70%	75%	80%	85%	90%	95%	100%	
0.025 m overburden depth																						
Geo-material	1	0.0914	0.0859	0.0806	0.0754	0.0703	0.0652	0.0602	0.0553	0.0505	0.0459	0.0412	0.0366	0.0321	0.0275	0.0232	0.0189	0.0148	0.0110	0.0073	0.0037	0.0000
	2	0.2033	0.1920	0.1811	0.1704	0.1495	0.1445	0.1392	0.1290	0.1188	0.1087	0.0987	0.0888	0.0789	0.0691	0.0592	0.0494	0.0395	0.0296	0.0198	0.0099	0.0001
	3	0.2443	0.2321	0.2200	0.2079	0.1957	0.1836	0.1715	0.1593	0.1472	0.1351	0.1229	0.1108	0.0987	0.0866	0.0744	0.0623	0.0502	0.0380	0.0259	0.0138	0.0016
	4	0.2733	0.2596	0.2460	0.2324	0.2187	0.2051	0.1914	0.1778	0.1641	0.1505	0.1369	0.1232	0.1096	0.0959	0.0823	0.0687	0.0550	0.0414	0.0277	0.0141	0.0005
POP	1	0.0754	0.0696	0.0642	0.0594	0.0549	0.0506	0.0466	0.0430	0.0394	0.0360	0.0326	0.0293	0.0260	0.0227	0.0195	0.0163	0.0131	0.0098	0.0066	0.0034	0.0002
Basalt	1	0.0201	0.0191	0.0181	0.0171	0.0161	0.0151	0.0141	0.0132	0.0122	0.0112	0.0102	0.0092	0.0082	0.0072	0.0062	0.0052	0.0042	0.0032	0.0022	0.0013	0.0003
	2	0.0302	0.0287	0.0272	0.0256	0.0241	0.0227	0.0212	0.0197	0.0182	0.0167	0.0152	0.0137	0.0122	0.0107	0.0092	0.0077	0.0062	0.0047	0.0032	0.0017	0.0002
	3	0.0411	0.0389	0.0367	0.0346	0.0324	0.0304	0.0283	0.0263	0.0243	0.0223	0.0203	0.0183	0.0163	0.0143	0.0122	0.0102	0.0082	0.0062	0.0042	0.0022	0.0002
	4	0.0598	0.0598	0.0538	0.0509	0.0479	0.0449	0.0419	0.0390	0.0360	0.0330	0.0300	0.0271	0.0241	0.0211	0.0181	0.0151	0.0122	0.0092	0.0062	0.0032	0.0003

Table 9 Comparison of deformation in different rocks for 0.05 m diameter *Unlined* tunnel having 0.035 m overburden depth ($\times 10^{-2}$ m) to understand the effect of pressure in terms of percentage reduction of UCS

Rock	0%	5%	10%	15%	20%	25%	30%	35%	40%	45%	50%	55%	60%	65%	70%	75%	80%	85%	90%	95%	100%	
0.035 m overburden depth																						
Geo-material	1	0.0866	0.0809	0.0754	0.0700	0.0646	0.0596	0.0545	0.0496	0.0450	0.0407	0.0364	0.0324	0.0285	0.0246	0.0210	0.0173	0.0138	0.0103	0.0069	0.0035	0.0003
	2	0.1799	0.1707	0.1615	0.1524	0.1343	0.1294	0.1254	0.1164	0.1075	0.0985	0.0896	0.0806	0.0717	0.0627	0.0538	0.0448	0.0359	0.0269	0.0180	0.0090	0.0001
	3	0.2113	0.2009	0.1904	0.1799	0.1694	0.1589	0.1484	0.1379	0.1274	0.1169	0.1064	0.0959	0.0855	0.0750	0.0645	0.0540	0.0435	0.0330	0.0226	0.0121	0.0016
	4	0.2378	0.2259	0.2141	0.2022	0.1903	0.1785	0.1666	0.1547	0.1428	0.1310	0.1191	0.1072	0.0954	0.0835	0.0716	0.0598	0.0479	0.0360	0.0242	0.0123	0.0004
POP	1	0.0590	0.0557	0.0525	0.0494	0.0463	0.0433	0.0403	0.0374	0.0345	0.0316	0.0288	0.0259	0.0230	0.0202	0.0173	0.0145	0.0116	0.0087	0.0059	0.0030	0.0001
Basalt	1	0.0175	0.0166	0.0152	0.0149	0.0140	0.0132	0.0123	0.0114	0.0106	0.0097	0.0089	0.0080	0.0071	0.0063	0.0054	0.0046	0.0037	0.0028	0.0021	0.0012	0.0003
	2	0.0267	0.0253	0.0240	0.0227	0.0214	0.0201	0.0187	0.0174	0.0161	0.0148	0.0134	0.0121	0.0108	0.0095	0.0082	0.0068	0.0055	0.0042	0.0029	0.0016	0.0002
	3	0.0363	0.0345	0.0327	0.0309	0.0291	0.0273	0.0255	0.0237	0.0219	0.0201	0.0183	0.0164	0.0146	0.0128	0.0110	0.0092	0.0074	0.0056	0.0038	0.0021	0.0002
	4	0.0538	0.0511	0.0484	0.0457	0.0430	0.0404	0.0377	0.0350	0.0323	0.0297	0.0270	0.0243	0.0216	0.0190	0.0163	0.0136	0.0109	0.0083	0.0056	0.0029	0.0002

Table 10 Comparison of deformation in different rocks for 0.05 m diameter *Unlined* tunnel having 0.050 m overburden depth ($\times 10^{-2}$ m) to understand the effect of pressure in terms of percentage reduction of UCS

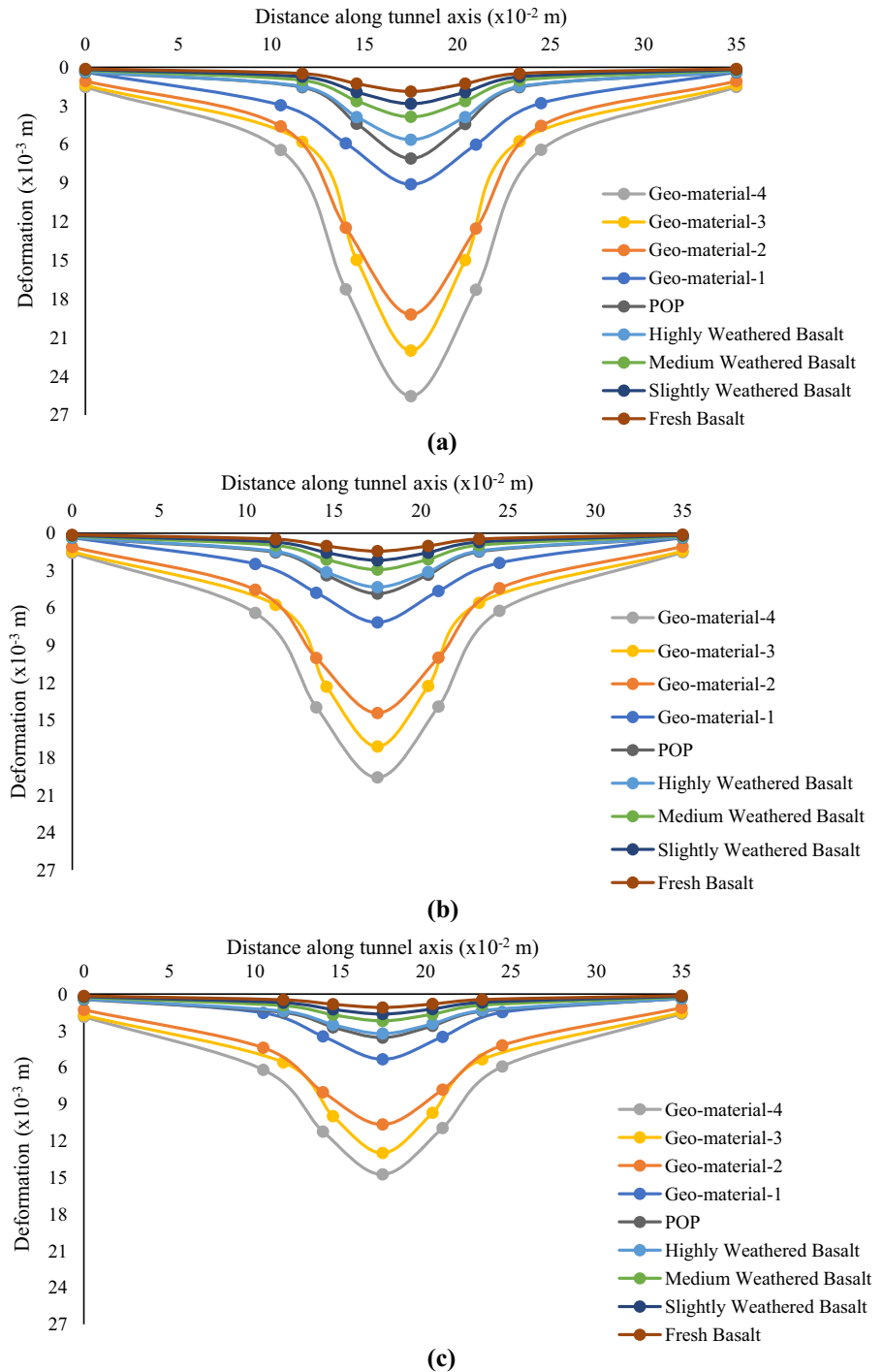
Rock	0%	5%	10%	15%	20%	25%	30%	35%	40%	45%	50%	55%	60%	65%	70%	75%	80%	85%	90%	95%	100%	
0.05 m overburden depth																						
Geo-material	1	0.0770	0.0715	0.0661	0.0612	0.0565	0.0520	0.0478	0.0437	0.0399	0.0361	0.0325	0.0289	0.0255	0.0221	0.0189	0.0157	0.0125	0.0094	0.0063	0.0031	0.0000
	2	0.1639	0.1556	0.1473	0.1390	0.1308	0.1225	0.1143	0.1061	0.0980	0.0898	0.0817	0.0735	0.0653	0.0572	0.0490	0.0409	0.0327	0.0245	0.0164	0.0082	0.0001
	3	0.1929	0.1833	0.1737	0.1642	0.1546	0.1450	0.1355	0.1259	0.1163	0.1068	0.0972	0.0877	0.0781	0.0685	0.0590	0.0494	0.0398	0.0303	0.0207	0.0111	0.0004
	4	0.2169	0.2061	0.1953	0.1845	0.1736	0.1628	0.1520	0.1411	0.1303	0.1195	0.1087	0.0979	0.0870	0.0762	0.0654	0.0546	0.0437	0.0329	0.0221	0.0113	0.0014
POP	1	0.0533	0.0505	0.0478	0.0450	0.0423	0.0396	0.0369	0.0342	0.0316	0.0289	0.0263	0.0237	0.0211	0.0184	0.0158	0.0132	0.0106	0.0080	0.0054	0.0028	0.0001
Basalt	1	0.0159	0.0152	0.0144	0.0136	0.0128	0.0120	0.0112	0.0105	0.0097	0.0089	0.0081	0.0073	0.0065	0.0057	0.0050	0.0042	0.0034	0.0026	0.0018	0.0010	0.0003
	2	0.0244	0.0232	0.0220	0.0208	0.0195	0.0183	0.0171	0.0159	0.0147	0.0135	0.0123	0.0111	0.0099	0.0087	0.0071	0.0063	0.0051	0.0038	0.0026	0.0014	0.0002
	3	0.0333	0.0316	0.0299	0.0283	0.0266	0.0250	0.0233	0.0217	0.0200	0.0183	0.0167	0.0150	0.0134	0.0117	0.0101	0.0084	0.0068	0.0051	0.0035	0.0018	0.0002
	4	0.0492	0.0467	0.0443	0.0418	0.0394	0.0369	0.0345	0.0320	0.0296	0.0271	0.0247	0.0223	0.0198	0.0174	0.0149	0.0125	0.0100	0.0076	0.0051	0.0027	0.0002

0.035 m and 0.05 m respectively, when the tunnel has a diameter of 0.05 m and pressure has value equal to the 100% of UCS. In the case of weathering of basalt, fresh basalt has been found as the safer rock while the

highly weathered basalt has maximum damage that has caused higher deformations in the tunnel.

Moreover, geo-material-1 experienced lesser deformations, and the geo-material-4 has a higher value of

Fig. 4 Deformation profile for the comparing of deformation in different rocks having 0.05 m tunnel diameter when magnitude of load equals the value of UCS, **a** 0.025 m overburden, **b** 0.035 m overburden, and **c** 0.05 m overburden for *lined* tunnel



deformation, which made the geo-material-4 as the most vulnerable case of geo-materials. Furthermore, it has been observed that the deformations in the tunnel reduced with an increase of overburden depth and reduction in the pressure on the loading patch. Therefore, the tunnels having higher overburden depth have lesser damage due to the applied load as compared to the tunnels having lesser overburden depth due to lithostatic condition. Also, it has been observed in Fig. 4a–c that deformations are concentrated in the vicinity of loading patch, and higher settlement has been observed for lower strength rock and geo-materials that surrounds the tunnel. The maximum magnitude of deformation is observed for the 0.025 m of overburden depth, and 0.050 m of overburden depth is the safer case for each diameter and weathering stage of rock and geo-material.

The geo-materials have been used to simulate the different stages of weathering at a laboratory level. Moreover, it has also proved an essential tool for understanding the relationship between the behaviour of different weathering stages of rock/geo-material for varying static loading conditions. Figure 5 shows the deformation profiles of different weathering stages of rock and four different geo-materials considered in the present study have been plotted for 0.025 m, 0.035 m and 0.050 m of overburden depth in case of unlined tunnels. It has been observed that the deformation is directly proportional to the degree of weathering and physical strength of rocks and geo-materials. In case of fresh weathering stage, the deformation has a lesser magnitude. Therefore, tunnels constructed in freshly weathered rock/geo-material has higher serviceability. Moreover, the highly weathered basalt and geo-material-4 have higher deformations due to its lower strength in comparison to fresh, slight and medium weathering stages. Therefore, the highly weathered basalt and geo-material-4 have lower safety and serviceability. The deformation varies linearly with the degree of weathering. However, the deformation increases exponentially in case of the highly weathered stage. Moreover, the depth of settlement at the ground is directly related to the degree of weathering, but it is inversely proportional to the overburden depth. Therefore, the maximum deformation occurred in the mid-section of the tunnel in the proximity of the loading area as observed in Fig. 5.

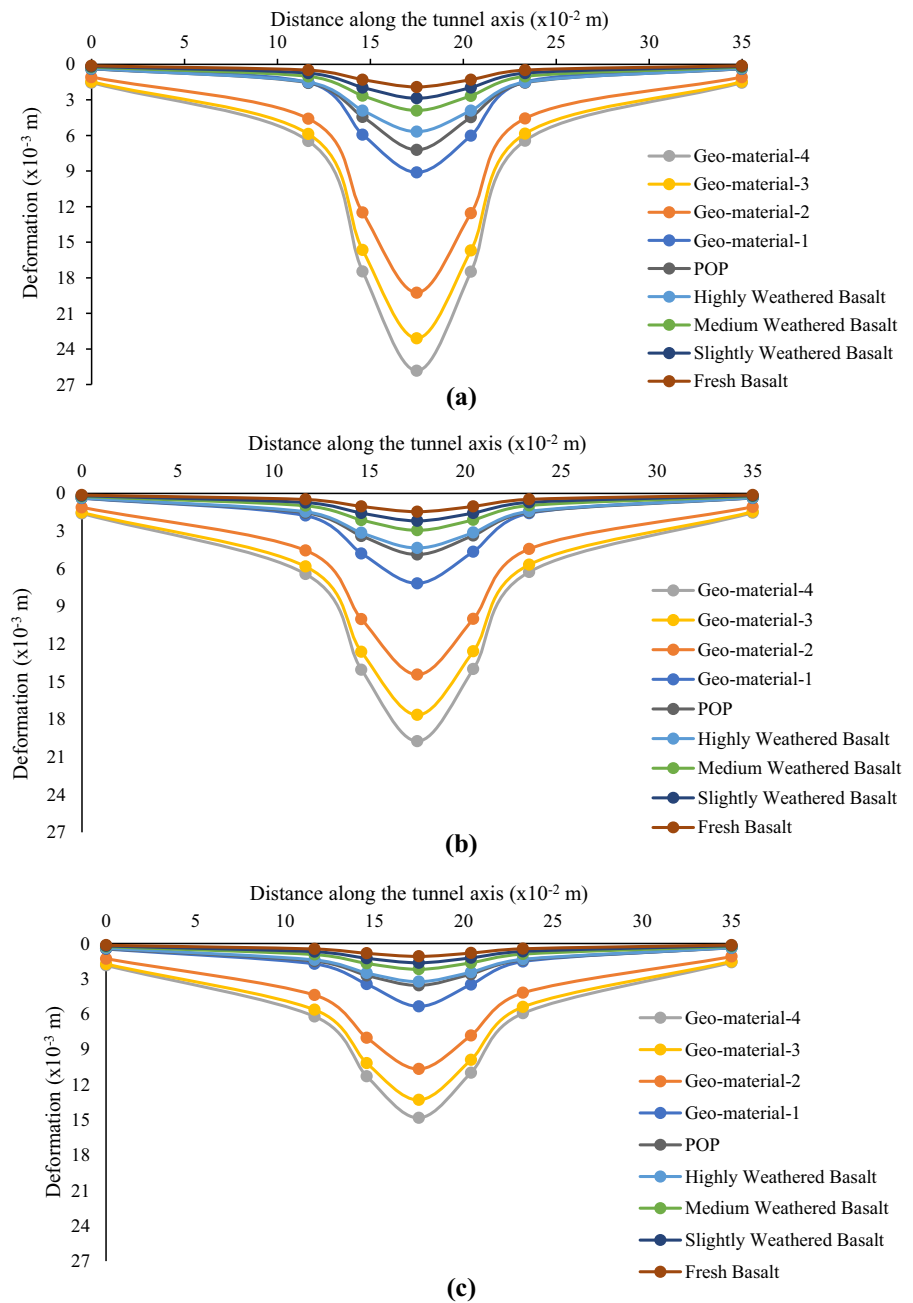
Figure 6 shows the longitudinal deformation profile of the tunnel to understand the effect of varying

diameter and variation of an overburden depth on the stability. The POP has been considered in the present case to compare the deformation profile for varying diameter and overburden depth of the lined and unlined tunnels. Since the POP is the readily available material that can be used in the laboratory to prepare the small-scaled models for testing, therefore, it has been considered in the present case. Figure 6a has been plotted for the lined tunnel constructed in different diameters and overburden depths of the tunnels. It was observed that the deformation in the tunnel increases with the increase in the diameter but decreases with an increase in an overburden depth of the tunnel. Therefore, an optimal combination of diameter and the overburden depth results in the construction of a safer and stable tunnel. Similarly, Fig. 6b has been plotted for unlined tunnels, which shows similar trends for various cases of diameters and overburden depths of the unlined tunnel. It has been observed that tunnel having 0.050 m of overburden depth is the most stable case for lined and unlined tunnels. Also, the change in diameter of the tunnel has a lesser effect in the case of 0.050 m of overburden depth. Moreover, the deformations are concentrated in the middle of the tunnel, i.e., 12 m of length, which varies with the weathering and magnitude of a load from loading patch. Therefore, the magnitude and area of loading have a significant effect on the extent of deformations in the lined and unlined tunnel.

Figure 7 shows the deformation profile of the lined tunnel having 0.025 m diameter and 0.025 m overburden depth. It has been observed that the deformation magnitude increase with the increase in the magnitude of pressure, which corresponds to the less percentage reduction of the UCS values. Moreover, the decrease in the magnitude of deformation has a uniform pattern along the length of the tunnel. Therefore, the linear variation has been observed between the percentage reduction in the magnitude of pressure and the deformations in the tunnel from Fig. 7. The maximum deformation is observed for 0% reduction in the magnitude of pressure, i.e., the value of UCS of rock/geomaterial surrounding the tunnel.

Figure 8 shows the deformation profile along the transverse axis for lined tunnel having 0.035 m of diameter and 0.035 m of overburden depth for four different deformation zones. The zones considered in the present study are Zone 1, Zone 2, Zone 3 and Zone 4 for the cases of fresh, slightly weathered, medium

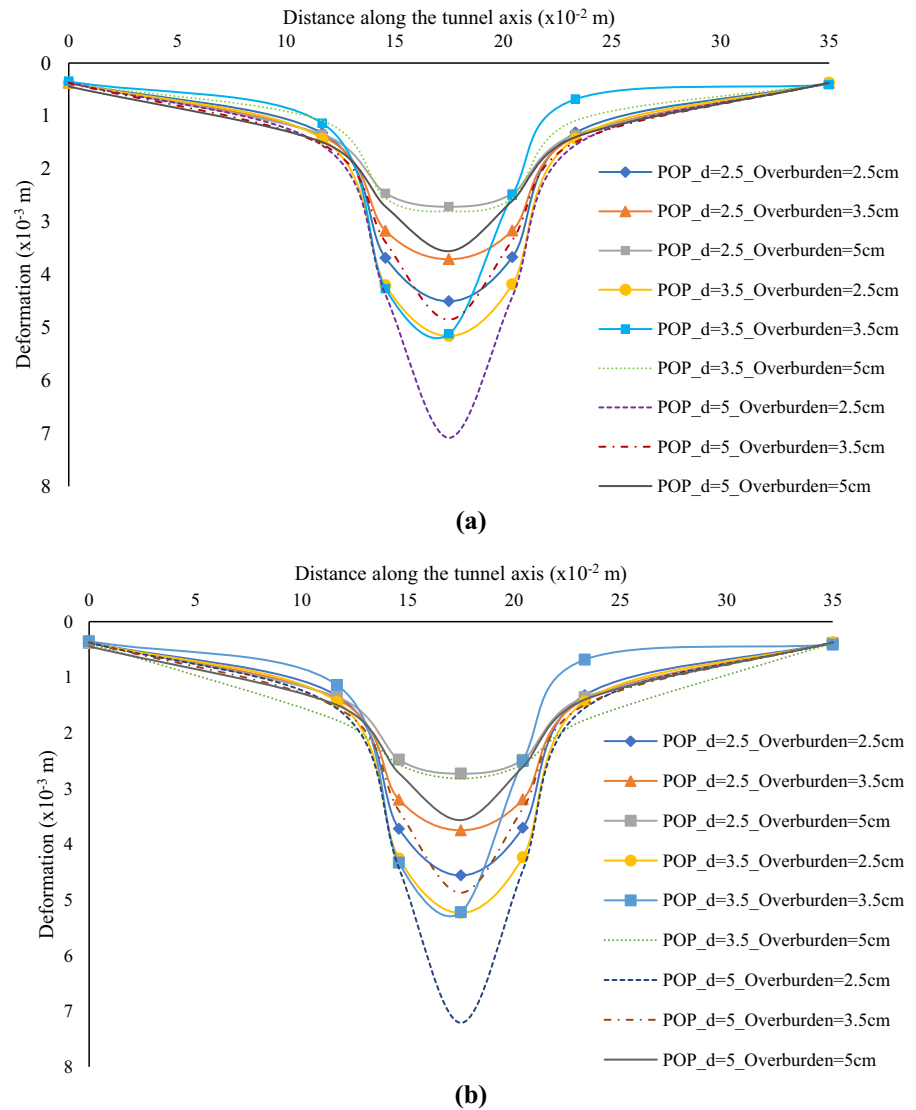
Fig. 5 Deformation profile for the comparing of deformation in different rocks having 0.05 m tunnel diameter when load has magnitude equal to UCS, **a** 0.025 m overburden, **b** 0.035 m overburden, and **c** 0.05 m overburden for *unlined* tunnel



weathered and highly weathered stages of basalt rock and geo-material-1, 2, 3, and 4. The different zones have been considered for four different locations along the length of the tunnel. Zone 1 corresponds to the center of the tunnel whereas Zone 2, Zone 3, and Zone 4 have been considered at a distance of 0.03 m, 0.06 m, and 0.09 m respectively, from the center of the tunnel. Moreover, these zones represent the “Zone

of Influence” for different rocks and geo-materials considered in the static loading study. It has been observed that the value of deformation decreases from Zone 1 to Zone 4, since the Zone 1 has been plotted at the centre of a tunnel. In Zone 1, the lesser area has been subjected to deformation, and small length experiences higher damage, however, in other cases of deformation zones, more considerable area

Fig. 6 Deformation profile for comparison of different overburden depth and diameter of tunnel having POP surrounding for **a** *Lined* tunnel, and **b** *Unlined* tunnel



experiences damage. Furthermore, the increasing depth of settlement has been observed with an increase in the degree of weathering in the present case.

Figure 9 shows the contour of Mises stress for different cases of lined and unlined tunnels constructed in the various rocks and geomaterials having 0.035 m of diameter and 0.035 m of overburden depth. This figure has been plotted for the comparison of Mises stresses at different stages of weathered basalt, four geo-materials and POP resulted due to the pressure (pressure = UCS) applied from the loading patch. It has been observed from Fig. 9, that the magnitude of Mises stresses increases with an increase in the degree of weathering. Moreover, it has been

observed that the stress increases by 48.5%, and 54% when the degree of weathering increases from fresh to slightly weathered, and slightly weathered to medium weathered basalt, respectively. Furthermore, the maximum change in the value of mises stress of 79.6% has been observed as the degree of weathering increases from medium to highly weathered basalt. The Mises stresses in case of geo-material 1, 2, 3 and 4 has a magnitude of 1.95 MPa, 10.39 MPa, 70.46 MPa and 80.47 MPa respectively. Also, the geo-material 4 has 41.27 times higher magnitude of Mises stress than geo-material 1, and the POP has the value of mises stress equal to 4.90 MPa.

Figures 10 and 11 shows the contours of mises stresses for the unlined tunnels in case of different weathering stages of basalt and geo-materials. The value of the Mises stress increases slightly in the present case. However, the unlined and lined tunnels have shown similar patterns of contours. The maximum magnitude of Mises stress has been found as 0.678 MPa, 1.41 MPa, 2.58 MPa, and 3.24 MPa for the fresh, slightly, medium and highly weathered stages of basalt respectively and 2.30 MPa, 12.01 MPa, 70.21 MPa, and 80.61 MPa in case of geo-material 1, 2, 3 and 4 respectively. The magnitude of Mises stress increases by 2-times, 1.83-times and 1.26-times when the weathering stage increases from fresh to slightly weathered, slightly weathered to medium weathered, medium weathered to highly weathered basalt. The different geomaterials considered in this study have also shown a similar pattern of escalation in the magnitude of Mises stress with the degree of weathering. Moreover, it has been observed that Mises stresses remain significant up-to-the invert of the tunnel. Therefore, the Mises stress has a higher magnitude around the area of influence of loading patch and its magnitude also reduces with increase in the distance away from the center of the tunnel. Also, it has been observed based on the values of Mises stresses that the overall stability of the tunnel is significantly influenced due to weathering.

Fig. 7 Deformation profile for 0.025 m diameter lined tunnel having 0.025 m overburden depth for different loading conditions having magnitude equal to the percentage reduction of UCS value

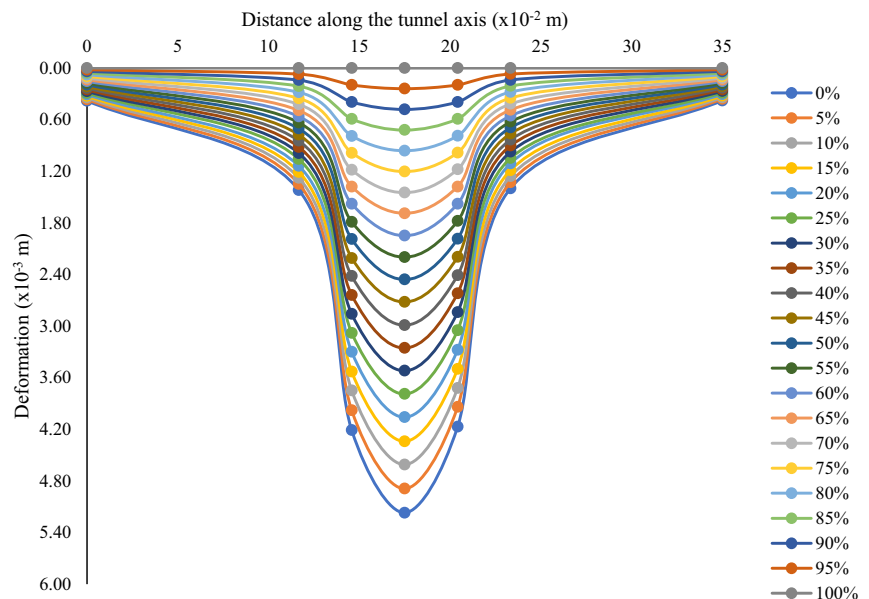
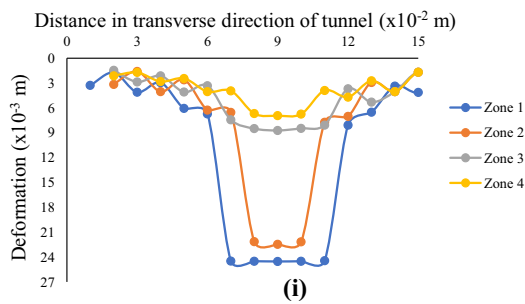
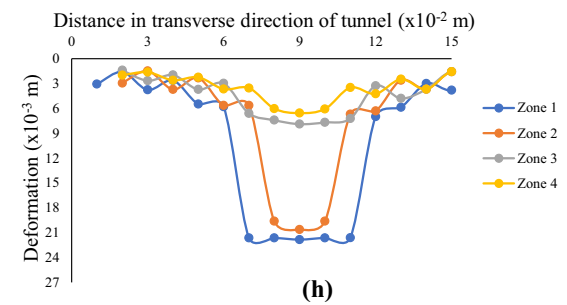
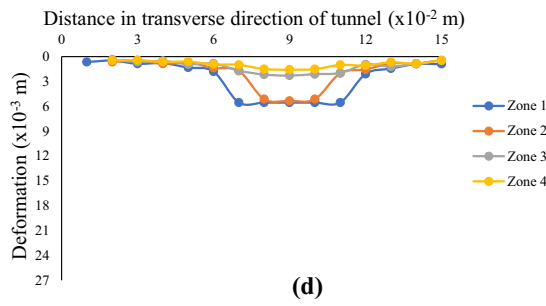
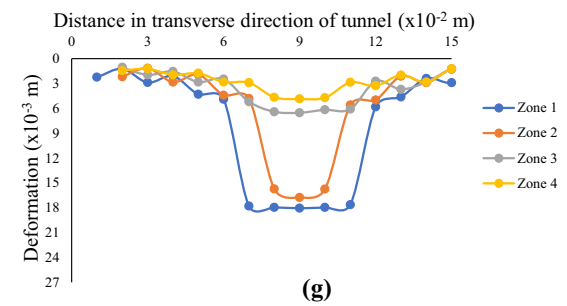
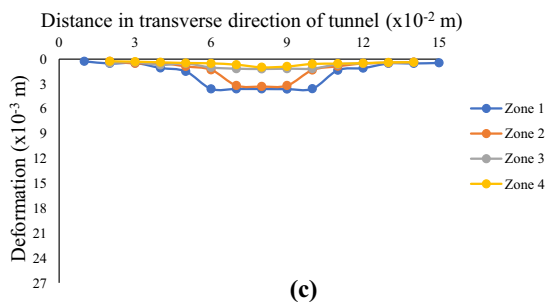
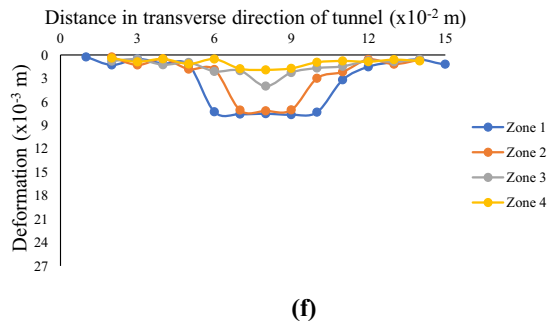
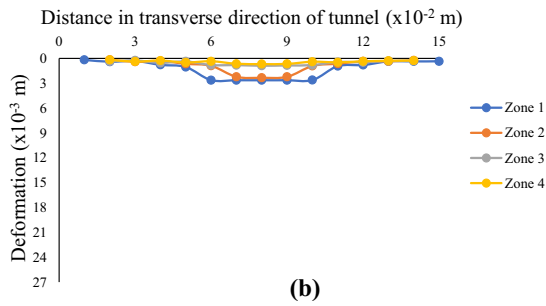
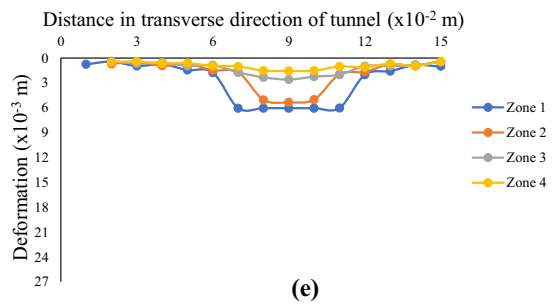
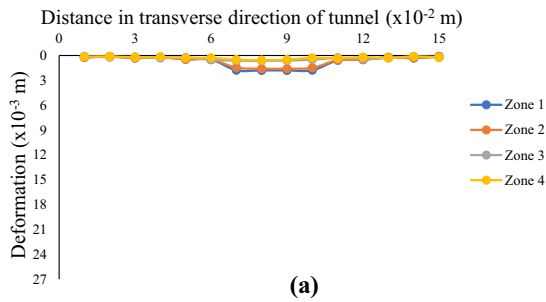
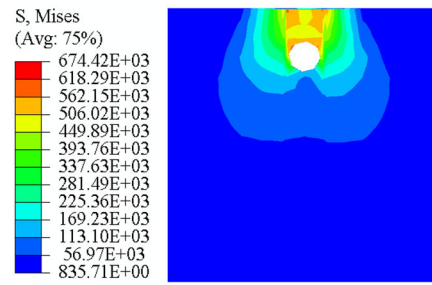
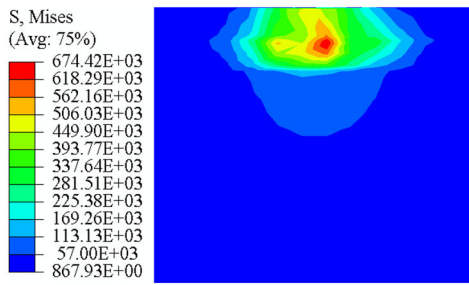


Fig. 8 Deformation profile of lined tunnel having 3.5 cm diameter and 3.5 cm overburden for different deformations zones along transverse direction of the tunnel for **a** Fresh Basalt, **b** Slightly Weathered Basalt, **c** Medium Weathered Basalt, **d** Highly Weathered Basalt, **e** POP, **f** Geo-material-1, **g** Geo-material-2, **h** Geo-material-3 and **i** Geo-material-4

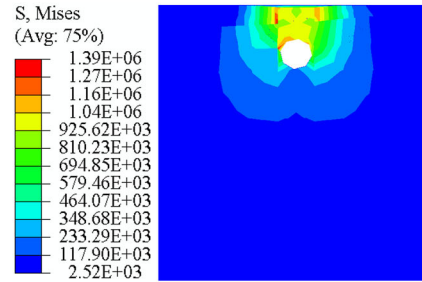
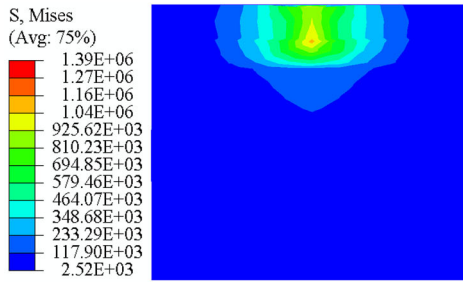
5 Analytical Study

In this section, an analytical equation has been proposed for the assessment of the deformation profiles of different rocks and geo-materials. The proposed equation has been derived through the curve fitting method available in the MATLAB programming tool (Martinez and Martinez 2007). The curve fitting method has been used to develop an equation for the data obtained from the analyses of different cases of rocks and geo-materials when overburden depth and diameter of the tunnel is 0.050 m and 0.050 m in dimensions. Moreover, the curve fitting method is readily available as already developed application in MATLAB programming tool. The data for the x -axis and y -axis was introduced in the application, where the horizontal axis represents the length of the tunnel and vertical axis represents the magnitude of deformation. The error reduced after several iterations, and Eq. (14) was obtained for plotting the deformation profile along the length of the tunnel. Moreover, dimensional analysis has been

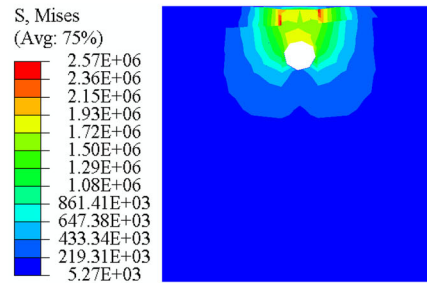
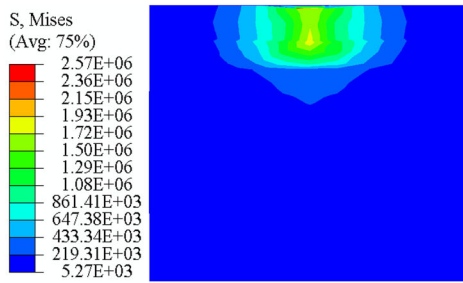




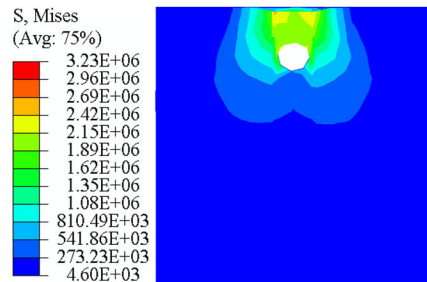
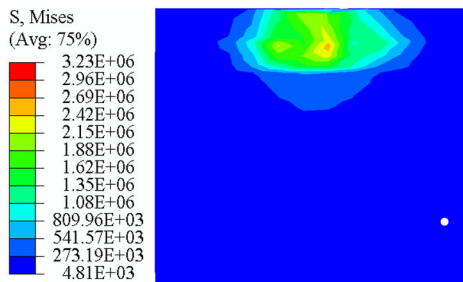
(a)



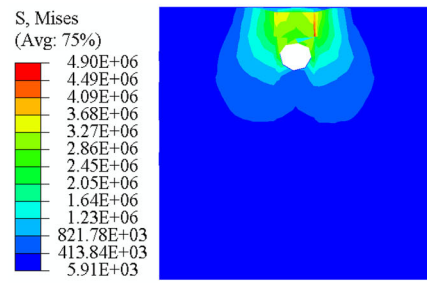
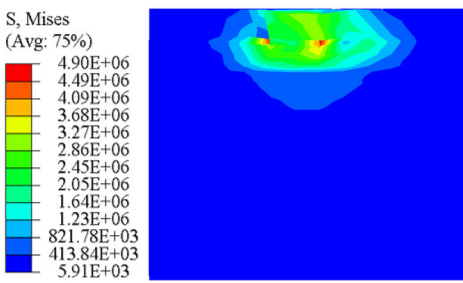
(b)



(c)



(d)



(e)

◀ **Fig. 9** Mises stress contours for different *lined* rock tunnels having 0.035 m diameter and 0.035 m of overburden depth, **a** Fresh Basalt, **b** Slightly Weathered Basalt, **c** Medium Weathered Basalt, **d** Highly Weathered Basalt, **e** Plaster of Paris, **f** Geo-material-1, **g** Geo-material-2, **h** Geo-material-3, and **i** Geo-material-4

carried out, and a constant was introduced, “a” as shown in Eq. (15). The deformation profile for the tunnel can be obtained by using-

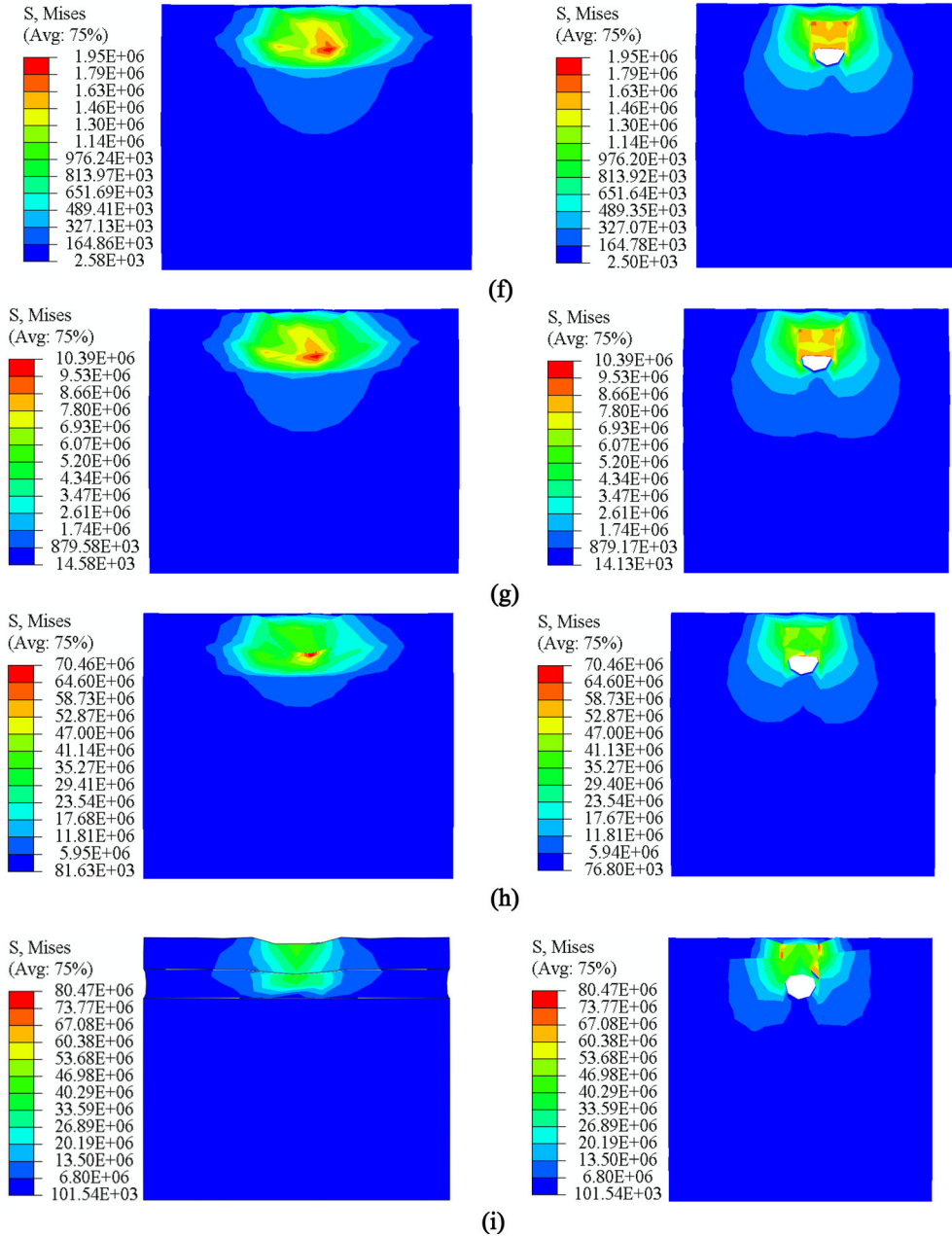


Fig. 9 continued

Deformation at the center of tunnel ($\times 10^{-2}$)

$$= a \times \left\{ \exp \left[- \left(\frac{x - 17.4}{7.42} \right)^2 \right] \right\} \quad (14)$$

where x = the half-length of the tunnel (in $m \times 10^{-2}$),
 a = constant, which is given as

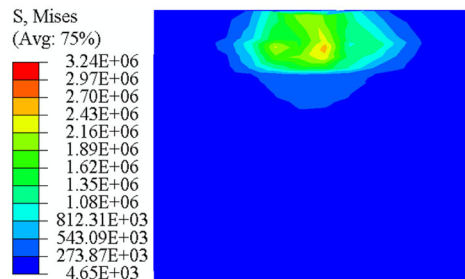
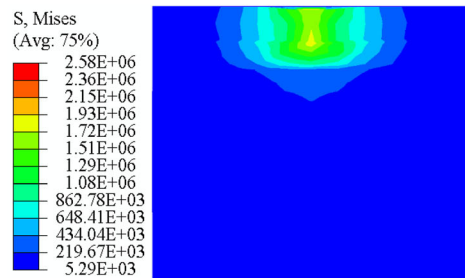
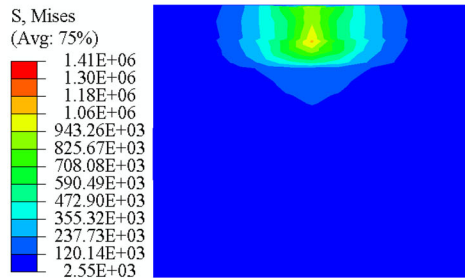
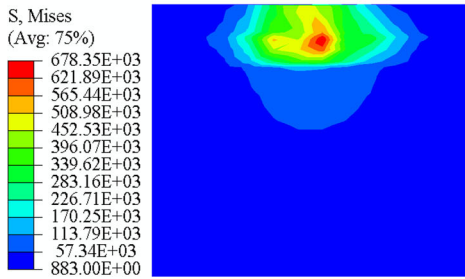


Fig. 11 Mises stress contour for different *unlined* rock tunnels having 0.035 m diameter and 0.035 m of overburden depth, **a** Plaster of Paris, **b** Geo-material-1, **c** Geo-material-2, **d** Geo-material-3, and **e** Geo-material-4

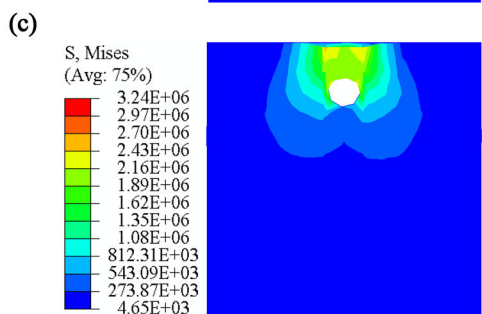
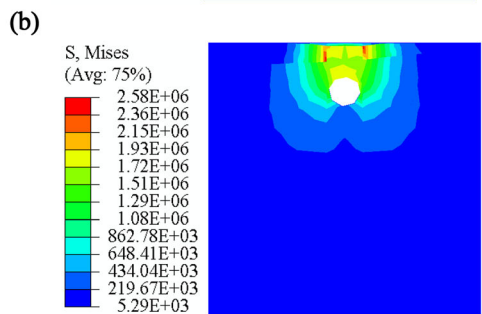
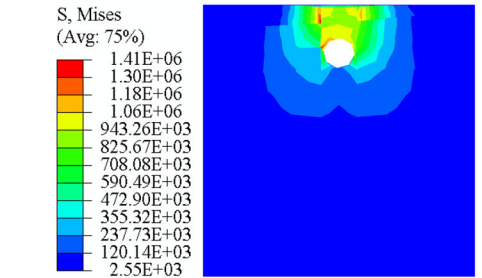
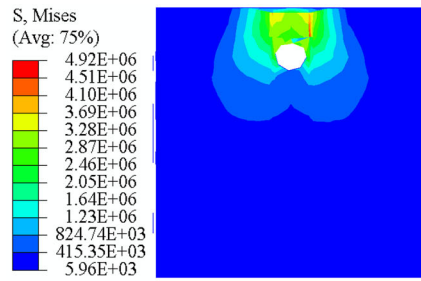
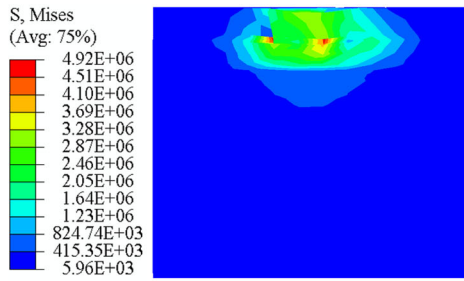
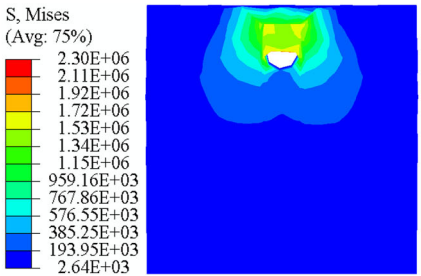
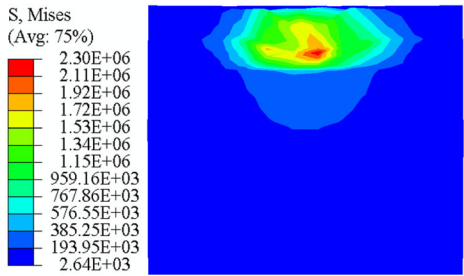


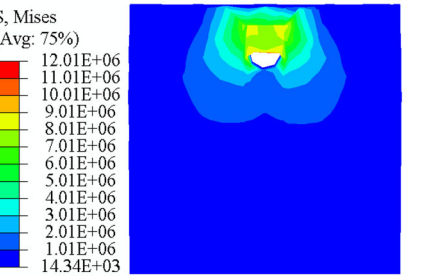
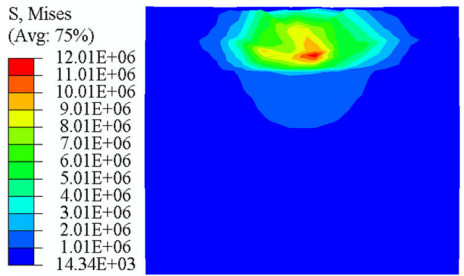
Fig. 10 Mises stress contour for different *unlined* rock tunnels having 0.035 m diameter and 0.035 m of overburden depth, **a** Fresh Basalt, **b** Slightly Weathered Basalt, **c** Medium Weathered Basalt, **d** Highly Weathered Basalt



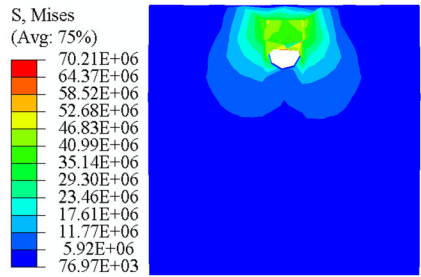
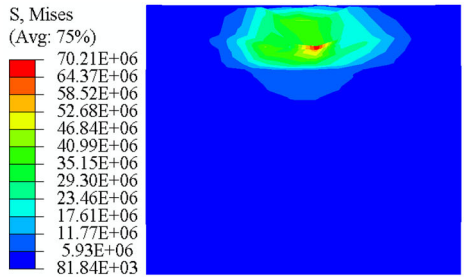
(a)



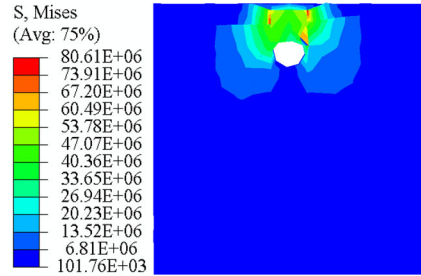
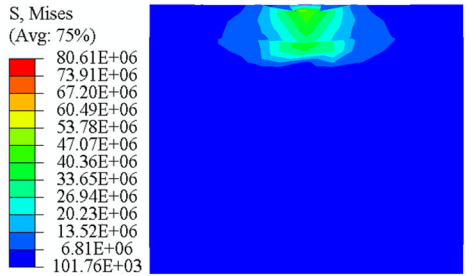
(b)



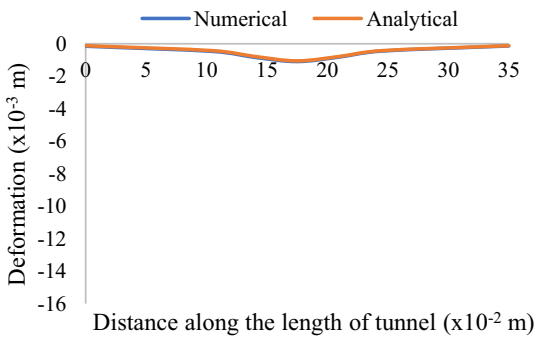
(c)



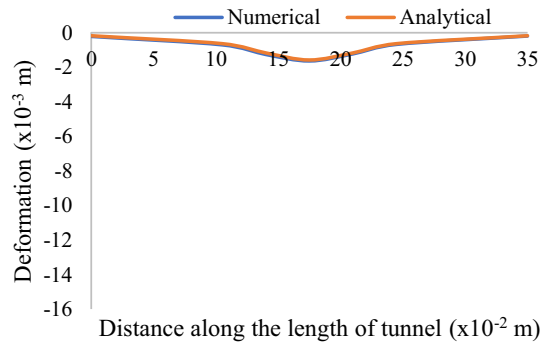
(d)



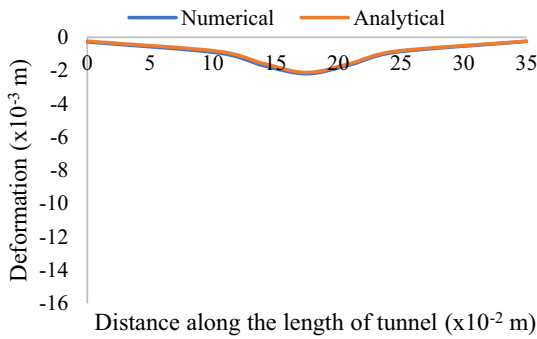
(e)



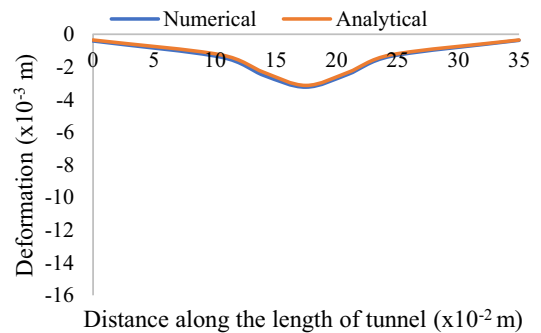
(a)



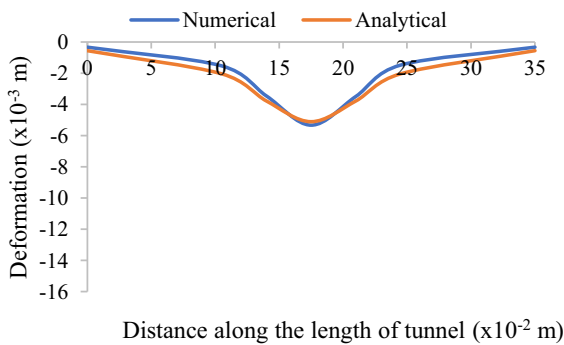
(b)



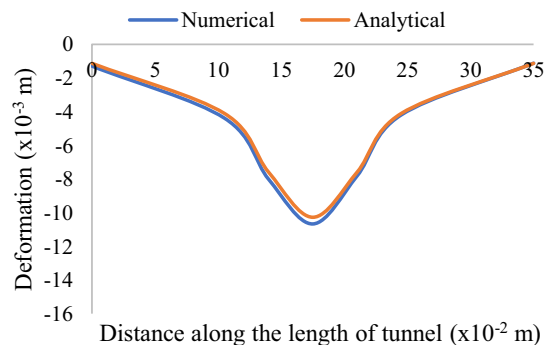
(c)



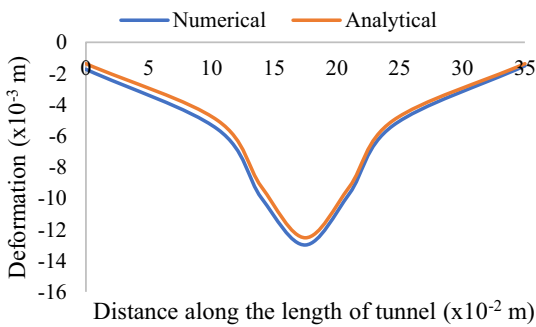
(d)



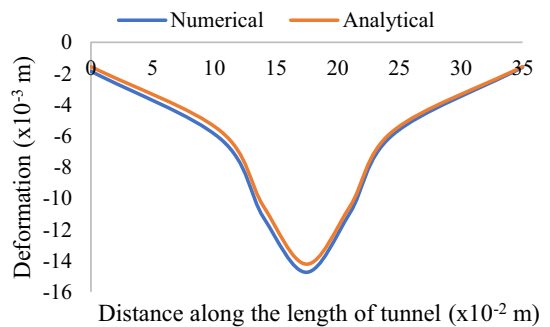
(e)



(f)



(g)



(h)

◀ **Fig. 12** Comparison of analytical and numerical results for different cases, **a** Fresh Basalt, **b** Slightly Weathered Basalt, **c** Medium Weathered Basalt, **d** Highly Weathered Basalt, **e** Geo-material-1, **f** Geo-material-2, **g** Geo-material-3 and **h** Geo-material-4

$$a = \frac{(-18.93(UCS) + 0.0221)}{((UCS)^2 - (1.222UCS) + 1.599)} \quad (15)$$

where UCS = Unconfined Compressive Strength of material surrounding the tunnel (in MPa)

Now, the deformation was calculated from the above Eqs. (14), (15) and substituted in Table 11 to give the final deformation profile in the present case. Moreover, the deformation profile of different rocks and geo-materials has been compared for the numerical and analytical case, which shows that the results from the analytical and numerical methods are in close vicinity. Therefore, the analytical method proposed in the present paper has been validated and can be used in a further investigation for static loading condition of tunnels.

The validity of the proposed Eqs. (14), (15) and Table 11 depends upon the type of loading, which must be similar to that considered in the present study. Therefore, the equation is applicable only for tunnels subjected to a static load. Also, the overburden depth to diameter ratio should be equal to unity as in the present case $\frac{Overburdendepth}{Diameteroftunnel} = \frac{0.050}{0.050}$ and the value of UCS should be higher than 1 MPa. In addition, the length of the tunnel section should be greater than 7-times the diameter of the tunnel.

An example:- Considering the case of “fresh basalt” having a C/D ratio as 1 (where, overburden depth = 0.050 m and diameter of tunnel = 0.050 m). From Table 3, fresh basalt has the UCS value of 172.55 MPa, and the plot has been obtained by using Eqs. (14), (15) and Tables 8, 9, 10, as shown in Fig. 12a. Similarly, the deformation profile has been

plotted for other cases of rocks and geo-materials in Fig. 12.

6 Conclusion

The present 3D finite element analysis has been carried out on urban tunnels having shallow depth using finite element software Abaqus. The following points can be concluded from the present study:

1. As the overburden depth increases from 0.025 m to 0.05 m the deformation in the tunnel and surrounding rockmass reduces. Since, increase in an overburden depth tends to lithostatic condition ($k_h/k_v = 1$), and thus, the stability of the tunnel increases with the increasing overburden depth.
2. It is observed that tunnel with a larger diameter is more prone to failure. Tunnel having a diameter of 0.025 m is safer than 0.05 m diameter tunnels. Tunnels with large diameter experiences sudden stress releases even at minimal loads and are highly unstable while tunnels with a smaller diameter almost act as a homogeneous medium with least chances of tunnel failure.
3. The weathering of the rock has a significant effect on the stability of the tunnel. With the increase in the weathering effect, shear strength parameters drop-down readily. It is observed that the value of unconfined compressive strength (UCS) and elastic modulus (E) decreases with the higher grade of weathered rocks, which finally leads to the instability of tunnels for same litho-static pressure.
4. It can be concluded that density, young’s modulus, friction angle and cohesion of the rock are inversely proportional to the deformation in the rock tunnel and the Poisson’s ratio of the rock is directly proportional to the deformations in the tunnel lining.
5. For comparison of engineering properties of geo-materials, the similar deformation has been observed for a percentage reduction in UCS by

Table 11 Data points for plotting the Deformation profile of different rocks

Location of Point (m × 10 ⁻²)	0.00	11.67	14.58	17.50	20.42	23.33	35.00
Deformation	0.11y	0.40y	0.74y	y	0.74y	0.40y	0.11y

50% in geo-material-1 and 85% in geo-material-4; similarly, 45% in Geo-material-2 and 60% in Geo-material-4. Similar is the case with percentage reduction by 60% in Geo-material-3 and 65% in Geo-material-4.

6. Also, the tunnel shows equal deformation for different rock masses, and the same deformation is obtained for a reduction pressure corresponding to the UCS value of 10% in fresh basalt, 40% in slightly weathered basalt, 55% in medium weathered basalt, and 70% in highly weathered basalt for 0.05 m diameter tunnel of 0.025 m overburden depth. For other cases also, geo-materials and basalt rocks were found to be related in term of percentage of UCS by the corresponding value of deformation.

It is quite cumbersome to find the maximum load that a tunnel can resist; however, the UCS value of geomaterials and rocks are predetermined. Therefore, the UCS value of different rocks and geo-materials are taken from the literature; hence, the loading has been varied in terms of UCS percentage. Moreover, the variation of load in terms of UCS provides an exhaustive parametric study for better understanding of the relation between load, deformations in the tunnel, different stages of weathering of rock, geomaterials surrounding the tunnel.

Compliance with ethical standards

Conflict of interest The authors declare that they have no potential conflict of interest.

References

- Abaqus (2014) ABAQUS user's manual, 6.14, Vers
- Ali Khan M, Sadique MR, Zaid M (2019) Effect of stratification on underground opening: a numerical approach. In: Advances in transportation engineering. Springer, pp 133–142. https://doi.org/10.1007/978-981-13-7162-2_11
- Athar MF, Zaid M, Sadique MR (2019) Stability of different shapes of tunnels in weathering stages of Basalt. In: Proceedings of national conference on advances in structural technology. NIT Silchar, pp 320–327
- Carranza-Torres C, Fairhurst C (1999) The elasto-plastic response of underground excavations in rock masses that satisfy the Hoek-Brown failure criterion. *Int J Rock Mech Min Sci* 36:777–809. [https://doi.org/10.1016/S0148-9062\(99\)00047-9](https://doi.org/10.1016/S0148-9062(99)00047-9)
- Chehade FH, Shahrou I (2008) Numerical analysis of the interaction between twin-tunnels: influence of the relative position and construction procedure. *Tunn Undergr Space Technol* 23:210–214. <https://doi.org/10.1016/j.tust.2007.03.004>
- De Buhan P, Cuvillier A, Dormieux L, Maghous S (1999) Face stability of shallow circular tunnels driven under the water table: A numerical analysis. *Int J Numer Anal Meth Geomech* 23:79–95. [https://doi.org/10.1002/\(SICI\)1096-9853\(199901\)23:1%3c79:AID-NAG960%3e3.0.CO;2-T](https://doi.org/10.1002/(SICI)1096-9853(199901)23:1%3c79:AID-NAG960%3e3.0.CO;2-T)
- Fakhimi A, Azhdari P, Kimberley J (2018) Physical and numerical evaluation of rock strength in Split Hopkinson Pressure Bar testing. *Comput Geotech* 102:1–11. <https://doi.org/10.1016/j.compgeo.2018.05.009>
- Fuenkajorn K, Phueakphum D (2010) Physical model simulation of shallow openings in jointed rock mass under static and cyclic loadings. *Eng Geol* 113:81–89. <https://doi.org/10.1016/j.enggeo.2010.03.003>
- Gahoi A, Zaid M, Mishra S, Rao KS (2017) Numerical analysis of the tunnels subjected to impact loading. In: 7th Indian rock conference, (IndoRock2017). Indorock2017, New Delhi
- Gao C, Li S, Wang J et al (2018) The risk assessment of tunnels based on grey correlation and entropy weight method. *Geotech Geol Eng* 36:1621–1631. <https://doi.org/10.1007/s10706-017-0415-5>
- Gioda G, Cividini A (1996) Numerical methods for the analysis of tunnel performance in squeezing rocks. *Rock Mech Rock Eng* 29:171–193. <https://doi.org/10.1007/BF01042531>
- Gupta AS (1997) Engineering behavior and classification of weathering rock. Indian Institute of Technology Delhi, Delhi
- Jia P, Tang CA (2008) Numerical study on failure mechanism of tunnel in jointed rock mass. *Tunn Undergr Space Technol* 23:500–507. <https://doi.org/10.1016/j.tust.2007.09.001>
- Jiang Y, Tanabashi Y, Li B, Xiao J (2006) Influence of geometrical distribution of rock joints on deformational behavior of underground opening. *Tunn Undergr Space Technol* 21:485–491. <https://doi.org/10.1016/j.tust.2005.10.004>
- Kasper T, Meschke G (2004) A 3D finite element simulation model for TBM tunnelling in soft ground. *Int J Numer Anal Meth Geomech* 28:1441–1460. <https://doi.org/10.1002/nag.395>
- Li S, Zhou Z, Li L et al (2013) Risk assessment of water inrush in karst tunnels based on attribute synthetic evaluation system. *Tunn Undergr Space Technol* 38:50–58. <https://doi.org/10.1016/j.tust.2013.05.001>
- Manouchehrian A, Cai M (2017) Journal of Rock Mechanics and Geotechnical Engineering Analysis of rockburst in tunnels subjected to static and dynamic loads. *Journal of Rock Mechanics and Geotechnical Engineering* 9:1031–1040. <https://doi.org/10.1016/j.jrmge.2017.07.001>
- Martinez W, Martinez A (2007) Computational statistics handbook with MATLAB
- Meguid MA, Saada O, Nunes MA, Mattar J (2008) Physical modeling of tunnels in soft ground: a review. *Tunn Undergr Space Technol* 23:185–198
- Mishra S (2019) Physical and Numerical Modeling of Tunnels Under Impact and Blast Loads. IIT Delhi

- Mishra S, Rao S, Gupta NK (2016) Effect of different loading conditions on tunnel lining in soft rocks. In: EUROCK 2016. Cappadocia (Turkey)
- Mishra S, Rao KS, Gupta NK, Kumar A (2017) Damage to shallow tunnels under static and dynamic loading. *Proc Eng* 173:1322–1329. <https://doi.org/10.1016/j.proeng.2016.12.171>
- Mishra S, Rao S, Gupta NK, Kumar A (2018) Damage to shallow tunnels in different geomaterials under static and dynamic loading. *Thin-Walled Struct* 126:138–149
- Mishra S, Kumar A, Rao KS, Gupta NK (2020) Experimental and numerical investigation of the dynamic response of tunnel in soft rocks. *Structures*. <https://doi.org/10.1016/j.istruc.2020.08.055>
- Moussaiefa N, Sharifzadehb M, Sahriarc K, Khosravia MH (2019) A new classification of failure mechanisms at tunnels in stratified rock masses through physical and numerical modeling. *Tunn Undergr Space Technol* 91:103017. <https://doi.org/10.1016/j.tust.2019.103017>
- Moyo T, Stacey TR (2012) Mechanisms of rock bolt support in jointed rock masses. In: Deep mining. Perth, Australia
- Naqvi MW, Zaid M, Sadique MR, Alam MM (2017) Dynamic analysis of rock tunnels considering joint dip angle: a finite element approach. In: 13th international conference on vibration problems. Indian Institute of Technology Guwahati, INDIA
- Naqvi MW, Akhtar MF, Zaid M, Sadique MR (2020) Effect of superstructure on the stability of underground tunnels. *Transport Infrastruct Geotechnol*. <https://doi.org/10.1007/s40515-020-00119-6>
- Ouchi A, Pakalnis R, AGM-CIM TB (2004) Update of span design curve for weak rock masses. In: Proceedings of the 99th annual AGM-CIM conference. Edmonton, AB
- Sakurai S (1983) Displacement measurements associated with the design of underground openings. In: Proceedings of international symposium on field measurements in geomechanics. Zurich, pp 1163–1178
- Senent S, Jimenez R (2015) A tunnel face failure mechanism for layered ground, considering the possibility of partial collapse. *Tunn Undergr Space Technol* 47:182–192. <https://doi.org/10.1016/j.tust.2014.12.014>
- Shen B, Barton N (1997) The disturbed zone around tunnels in jointed rock masses. *Int J Rock Mech Min Sci* 34:117–125. [https://doi.org/10.1016/S1365-1609\(97\)80037-8](https://doi.org/10.1016/S1365-1609(97)80037-8)
- Song S, Li S, Li L et al (2019) Model test study on vibration blasting of large cross-section tunnel with small clearance in horizontal stratified surrounding rock. *Tunn Undergr Space Technol* 92:103013. <https://doi.org/10.1016/j.tust.2019.103013>
- Sterpi D, Cividini A (2004) A physical and numerical investigation on the stability of shallow tunnels in strain softening media. *Rock Mech Rock Eng* 37:277–298. <https://doi.org/10.1007/s00603-003-0021-0>
- Systemes D (2014) Abaqus 6.14 Documentation. Providence, RI: Dassault Systèmes
- Wang J, Li S, Li L et al (2019) Attribute recognition model for risk assessment of water inrush. *Bull Eng Geol Environ* 78:1057–1071. <https://doi.org/10.1007/s10064-017-1159-4>
- Zaid M, Rehan Sadique M (2021) Dynamic analysis of tunnels in western ghats of Indian Peninsula: effect of shape and weathering. In: Recent trends in civil engineering. Springer, Singapore, pp 763–776. https://doi.org/10.1007/978-981-15-5195-6_57
- Zaid M, Sadique MR (2020a) The response of rock tunnel when subjected to blast loading: finite element analysis. *Eng Rep*. <https://doi.org/10.1002/eng2.12293>
- Zaid M, Sadique MR (2020b) Effect of unconfined compressive strength of rock on dynamic response of shallow unlined tunnel. *SN Appl Sci*. <https://doi.org/10.1007/s42452-020-03876-8>
- Zaid M, Sadique MR (2020c) Blast resistant behaviour of tunnels in sedimentary rocks. *Int J Protect Struct*. <https://doi.org/10.1177/2041419620951211>
- Zaid M, Sadique MR (2020d) Numerical modelling of internal blast loading on a rock tunnel. *Advn Comput Des* 5:417–443. <https://doi.org/10.12989/acd.2020.5.4.417>
- Zaid M, Athar MF, Sadique MR (2019a) Effect of rock weathering on the seismic stability of different shapes of the tunnel. In: Indian geotechnical conference (IGC2019). SVNIT, Surat, India
- Zaid M, Mishra S, Rao KS (2019b) Stability of different shapes of himalayan tunnels under blast loading. In: 8th Indian rock conference. New Delhi, pp 375–380
- Zaid M, Shah IA, Farooqi MA (2019c) Effect of cover depth in unlined himalayan tunnel: a finite element approach. In: 8th Indian rock conference. new Delhi, pp 448–454
- Zaid M, Mishra S, Rao KS (2020a) Finite element analysis of static loading on urban tunnels. In: Madhavi Latha Gali, Raghuvveer Rao P (eds) Geotechnical characterization and modelling, 1st edn. Springer, Singapore, pp 807–823. https://doi.org/10.1007/978-981-15-6086-6_64
- Zaid M, Sadique MR, Alam MM, Samanta M (2020b) Effect of shear zone on dynamic behaviour of rock tunnel constructed in highly weathered granite. *Geomech Eng* 23:245. <https://doi.org/10.12989/GAE.2020.23.3.245>
- Zaid M, Talib A, Sadique MR (2021) Effect of joint orientation on the seismic stability of rock slope with transmission tower. In: Geohazards. Springer, pp 149–161. https://doi.org/10.1007/978-981-15-6233-4_11
- Zangerl C, Eberhardt E, Evans KF, Loew S (2008) Consolidation settlements above deep tunnels in fractured crystalline rock: part 2-Numerical analysis of the Gotthard highway tunnel case study. *Int J Rock Mech Min Sci* 45:1211–1225. <https://doi.org/10.1016/j.ijmms.2008.02.005>
- Zhao K, Bonini M, Debernardi D et al (2015) Computational modelling of the mechanised excavation of deep tunnels in weak rock. *Comput Geotech* 66:158–171. <https://doi.org/10.1016/j.compgeo.2015.01.020>

Publisher's Note Springer Nature remains neutral with regard to jurisdictional claims in published maps and institutional affiliations.